

1 **Co-location of the downdip end of seismic locking and**  
2 **the continental shelf break**

3 **Luca C. Malatesta<sup>1,2,3</sup>, Lucile Bruhat<sup>4</sup>, Noah J. Finnegan<sup>1</sup>, Jean-Arthur L.**  
4 **Olive<sup>4</sup>**

5 <sup>1</sup>Department of Earth and Planetary Sciences, University of California Santa Cruz, Santa Cruz,  
6 California, USA.

7 <sup>2</sup>Institute of Earth Surface Dynamics, University of Lausanne, Lausanne, Switzerland

8 <sup>3</sup>Earth Surface Process Modelling, GFZ German Research Center for Geosciences, Potsdam, Germany

9 <sup>4</sup>Laboratoire de Géologie, UMR 8538, École Normale Supérieure, PSL University, CNRS, Paris, France

10 **Key Points:**

- 11 • Shelf breaks at subduction margins lie above the seismic locking depth.  
12 • Spatial patterns of interseismic deformation are reflected in long-term subduction  
13 margin uplift.  
14 • The morphology of a subduction margin integrates deformation from hundreds  
15 of seismic cycles.

**Abstract**

Along subduction margins, the morphology of the near shore domain records the combined action of erosion from ocean waves and permanent tectonic deformation from the convergence of plates. We observe that at subduction margins around the globe, the edge of continental shelves tends to be located above the downdip end of seismic coupling on the megathrust (locking depth). Coastlines lie farther landward at variable distances. This observation stems from a compilation of well-resolved coseismic and interseismic coupling datasets. The permanent interseismic uplift component of the total tectonic deformation can explain the localization of the shelf break. It contributes a short wavelength gradient in vertical deformation on top of the structural and isostatic deformation of the margin. This places a hinge line between seaward subsidence and landward uplift above the locking depth. Landward of the hinge line, rocks are uplifted in the domain of wave-base erosion and a shelf is maintained by the competition of rock uplift and wave erosion. Wave erosion then sets the coastline back from the tectonically meaningful shelf break. We combine a wave erosion model with an elastic deformation model to show how the locking depth pins the location of the shelf break. In areas where the shelf is wide, onshore geodetic constraints on seismic coupling is limited and could be advantageously complemented by considering the location of the shelf break. Subduction margin morphology integrates hundreds of seismic cycles and could inform seismic coupling stability through time.

**1 Introduction**

The area of a subduction interface that is frictionally locked between earthquakes controls the size of megathrust ruptures (Aki, 1967; Mai & Beroza, 2000). Strain accumulation from partial locking of the plate interface produces interseismic deformation at the surface, which can be inverted to determine the extent of the locked region on the fault, following the widely used back slip model (Savage, 1983). This procedure has been used for decades to produce maps of locking, also referred to as coupling, over subduction zones (e.g. Yoshioka et al., 1993; Sagiya, 1999; Mazzotti et al., 2000; Nishimura et al., 2004; Simoes et al., 2004; Chlieh et al., 2008; Metois et al., 2012). However, due to the short duration of geodetic measurements, these inversions typically reflect a fraction of the earthquake cycle, which could be contaminated by transient slip events (Dragert et al., 2001; Obara, 2002), postseismic deformation from previous large earthquakes (e.g.

48 Trubienko et al., 2013; Sun et al., 2018), or deformation unrelated to the megathrust (like  
49 postglacial rebound, James et al., 2009). Because the locked region is typically offshore,  
50 it may also be poorly constrained simply due to the concentration of geodetic measure-  
51 ments on land. This problem is compounded by wide continental shelves (Wang & Tréhu,  
52 2016). Seafloor geodesy can overcome some of these problems, but remains uncommon  
53 (Bürgmann & Chadwell, 2014). Any progress toward better constraining the size of locked  
54 patches is an important goal for the seismotectonic community.

55 On land, tectonic geomorphology complements short duration geodetic and seis-  
56 mic records and provides a meaningful tectonic record that is often missing offshore (e.g.  
57 Valensise & Ward, 1991; Lavé & Avouac, 2001; Brooks et al., 2011). During the seismic  
58 cycle, crustal deformation is considered as almost entirely elastic and balanced by co-  
59 seismic deformation. But over geological time scales, herein *long-term* ( $> 10^5$  yrs), the  
60 small fraction of deformation that is anelastic and permanent would accumulate and con-  
61 tribute to mountain building (Avouac, 2003).

62 Among the little work that has linked submarine geomorphology and subduction  
63 zone deformation, Ruff and Tichelaar (1996) identified a correlation between the downdip  
64 end of subduction zone rupture and the position of the coastline. This correlation fits  
65 the Andean subduction particularly well, and Saillard et al. (2017) suggested that the  
66 distribution of anelastic interseismic deformation could explain it. However, the posi-  
67 tion of the coastline at active margins depends on several processes that are not tectonic  
68 in nature, the most important of which is the ever-varying sea level. The current loca-  
69 tion of the coastline is specific to a high-stand situation; at the last glacial maximum,  
70  $\sim 20$  ka, global sea level was at a low-stand that was on average  $\sim 125$  m lower than present  
71 level (Spratt & Lisiecki, 2016). The world’s coastlines were then all shifted seaward, e.g.  
72  $\sim 3$ – $25$  km along the Andes,  $\sim 5$ – $45$  km along North Honshu, or  $\sim 15$ – $45$  km along Cas-  
73 cadia, depending on the slope of the shelf (Ryan et al., 2009). Secondly, the coastline  
74 of an uplifting active margin is erosive in essence: its location depends on the compe-  
75 tition between wave erosion and uplift (Bradley & Griggs, 1976; Anderson et al., 1999).  
76 In short, coastlines are weak candidates to inform about tectonic processes as their lo-  
77 cations vary frequently due to non-tectonic factors. As a matter of fact, McNeill et al.  
78 (2000) and Booth-Rea et al. (2008) noted that, in Cascadia, the outer-arc high struc-  
79 ture marking the edge of the continental shelf lies approximately above the downdip end

80 of locking. The tectonic significance of active margin shelves thus merits to be investi-  
81 gated.

82 There is no unambiguous definition for *shelf* across geosciences communities. Here,  
83 we understand shelf in a geomorphological context, i.e., the submarine domain affected  
84 by wave-base erosion over cycles of low to high-stand, resulting in a more or less gen-  
85 tle platform no deeper than 200 m below modern sea level (Bouma et al., 1982). Con-  
86 trary to passive margins where the shelf break is a stratigraphic edifice whose location  
87 reflects the volume of sediment shed from continents (Bouma et al., 1982), the shelf break  
88 of a subduction forearc is often pinned by tectonic deformation (Seely & Dickinson, 1977;  
89 McNeill et al., 2000; Booth-Rea et al., 2008). Compressional and extensional strain caused  
90 by partial locking between the overriding and downgoing plates are its primary drivers  
91 (Fuller et al., 2006; Wang & Hu, 2006; Cubas et al., 2013; Noda, 2016). In fact, the shelf  
92 break has been referred to as *outer arc high*, *structural high*, or *outer high* (Seely & Dick-  
93 inson, 1977). The outer arc high is often set by a thrust (blind or not) and marks the  
94 upper limit of the continental slope, where rocks begin to experience wave base erosion  
95 (Seely & Dickinson, 1977; Anderson et al., 1999). Depending on its relative uplift rate,  
96 the outer-arc high is either the edge of an erosional platform or the seaward sill (some-  
97 times buried) of a forearc basin (Noda, 2016). Whether in a narrow erosive zone (e.g.  
98 the Andean subduction zone), or a complex domain with multiple deforming basins trapped  
99 behind the outer-arc (e.g. Cascadia), the shelf break is a clear topographic feature that  
100 is easily identifiable at almost all active margins regardless of their structure (Seely &  
101 Dickinson, 1977; Noda, 2016). That said, we acknowledge exceptions such as in the Alaska  
102 and the Colombia-Ecuador subduction zones where the foresets of a depositional system  
103 mark the edge of the shelf (Bouma et al., 1982).

104 Since the compilation by Ruff and Tichelaar (1996), advances in geodetic inversions  
105 for interseismic coupling and coseismic ruptures have allowed renewed scrutiny of po-  
106 tential relationships between subduction zone locking and coastal morphology. In this  
107 article, we repeat the work of Ruff and Tichelaar (1996) with additional data; first with  
108 well-resolved coseismic ruptures and second with solutions for both interseismic coupling  
109 and the extent of large coseismic ruptures. We observe that the edge of the continen-  
110 tal shelf is a better first-order predictor of the locking depth than the originally proposed  
111 coastline. To explore and illustrate the submarine geomorphic expression of the location  
112 of the locking depth, we then develop a model of wave erosion across a subduction mar-

113 gin where long-term vertical deformation is partly driven by the anelastic fraction of the  
 114 interseismic deformation. We show that the location of the shelf break can constrain the  
 115 extent of the locked region integrated over many earthquake cycles in subduction zones.

## 116 **2 Apparent co-location of shelf break with the downdip end of seis-** 117 **mic locking**

### 118 **2.1 Position of coseismic ruptures**

119 The amount of data constraining the downdip end of seismic ruptures and inter-  
 120 seismic coupling has increased in the two decades that followed the work of Ruff and Tichelaar  
 121 (1996), and warrants a new look at potential relations between landscape and seismo-  
 122 genic patterns. Figure 1 shows the outline of solutions for the downdip end of interseis-  
 123 mic coupling in Cascadia, and the downdip end of coseismic ruptures in Japan and Cen-  
 124 tral America. At the three locations, the locking depth is broadly located below the shelf  
 125 break. These sites have shelves of width varying from about 25 to 75 km (highlighted  
 126 by the 200 m depth contour line).

127 The same co-location pattern can be observed in a global compilation of the region-  
 128 ally largest coseismic ruptures (Figure 2). This representation compares the respective  
 129 distances between locking depth, shelf break, and coastline following and expanding on  
 130 the earlier work of Ruff and Tichelaar (1996). To recover the position of the downdip  
 131 end of coupling, we collected maps of large coseismic ruptures and interseismic coupling  
 132 for the major subduction systems. The downdip end of the coupled (using  $\sim 80\%$  cou-  
 133 pling as a threshold) and of the rupture patches were exported to Google Earth (*kml* file  
 134 available in the supplementary material). In each subduction system, relative positions  
 135 of the trench, the locking depth, the shelf break, and the coastline were measured along  
 136 three to six profiles normal to the margin. Survey profiles were positioned to capture vari-  
 137 ability in relative positions of the locking and morphological markers. The shelf break  
 138 is identified as the transition from the continental platform to the continental slope or,  
 139 in the absence of clear features, pinned at  $\sim 200$  m depth. For the sites where the shelf  
 140 break is set by a structural feature and not by stratigraphic foresets, we observe (Fig-  
 141 ure 2 inset) that the mean position of the shelf breaks lie 1.13 km seaward of the downdip  
 142 ends of rupture (10<sup>th</sup>/90<sup>th</sup> percentiles at -25.5/16 km), while the coastlines lie landward  
 143 at an average distance of 29.2 km (10<sup>th</sup>/90<sup>th</sup> percentiles at 1/54 km).

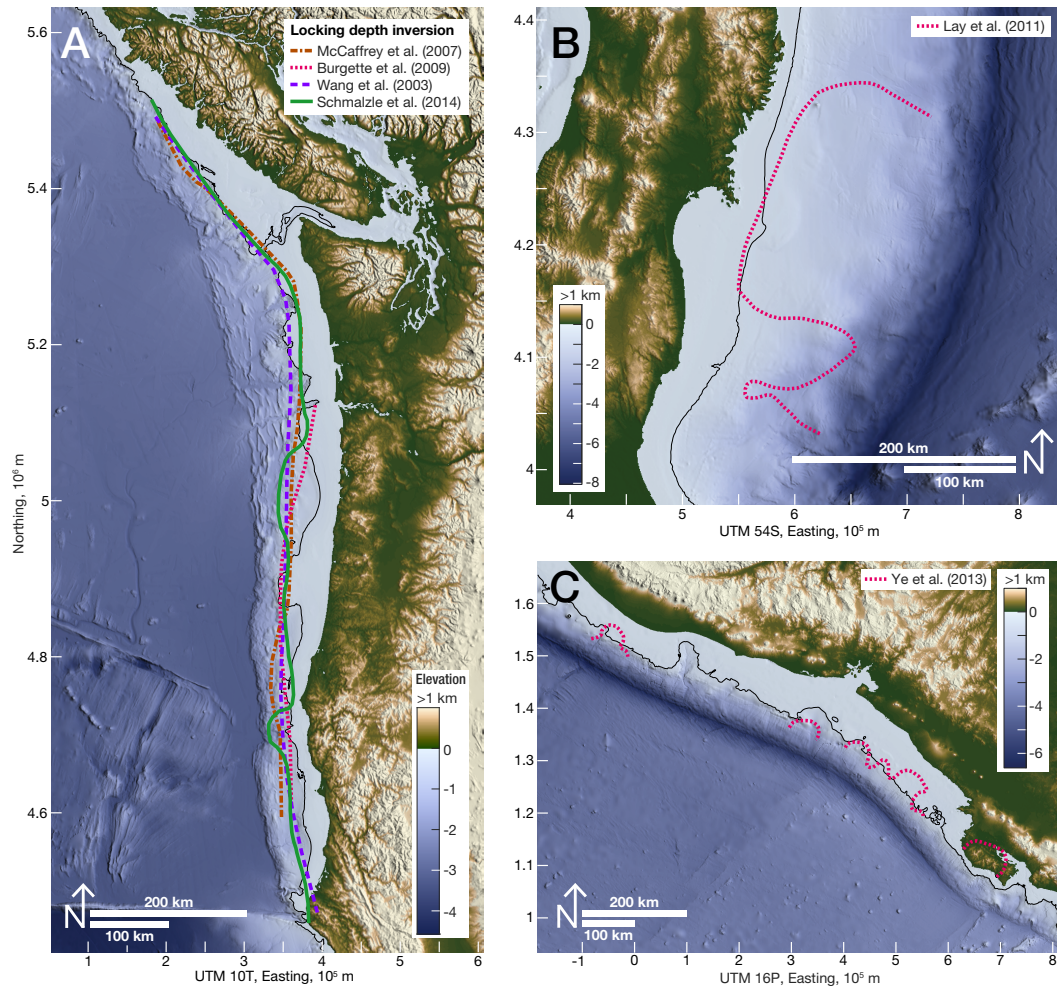


**Figure 1.** A: Solutions for the downdip end of interseismic coupling in Cascadia, derived from GPS (Wang et al., 2003; McCaffrey et al., 2007; Schmalzle et al., 2014) and road leveling and tide gauges measurements (Burgette et al., 2009). The locking depth is outlined for a value of  $\sim 80\%$  locking. B: Rupture extent of the  $M_w$  9.1 Tōhoku-Oki earthquake (Lay et al., 2011). C: Rupture extent (at  $\sim 0.5$  m displacement) of four Central American  $M_w > 7$  megathrust earthquakes (Ye et al., 2013). The downdip ends of coupling and ruptures follow the edge of the continental shelf and are removed from the coastline. The black contour indicates 200 m depth, a common approximation for the geomorphic shelf edge. Topographic data from Ryan et al. (2009); color map from Cramer (2018).

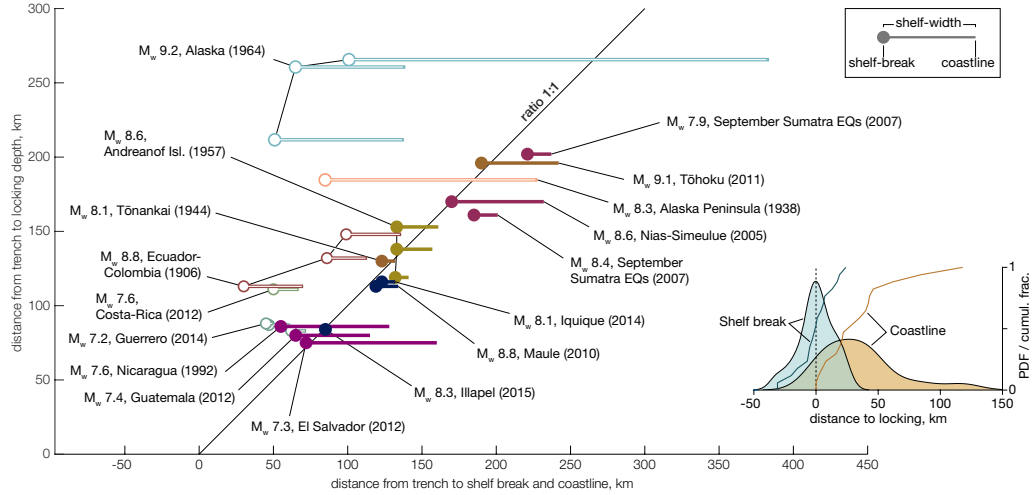


**Figure 2.** Position of the downdip edge of large megathrust earthquakes with respect to the local shelf break and coastline using the trench as origin (plot inspired by Ruff and Tichelaar (1996)). The inset kernel distribution shows the distance of shelf-edges and coastlines to the downdip edge of ruptures at sites marked with filled circles in the main plot (see text for rationale). Shelf breaks are tightly distributed around the locking depth at a mean distance of -1.13 km (10<sup>th</sup>/90<sup>th</sup> percentiles at -25.5/16 km) while coastlines are removed and spread landward from it at a mean distance of 29.2 km (10<sup>th</sup>/90<sup>th</sup> percentiles at 1/54 km). Sources are Sykes et al. (1981); Johnson (1998); Park et al. (2002); Cross and Freymueller (2007); Konca et al. (2008); Lay et al. (2011); Ye et al. (2013); Yue et al. (2014); Lay et al. (2014); Nocquet et al. (2014); Li et al. (2016).

## 2.2 Shelf break and locking depth from co- and interseismic surveys.

The compilation can be further expanded with the inclusion of solutions for interseismic locking that were developed with the advent of GPS monitoring (Larsen & Reilinger, 1992; Savage & Thatcher, 1992). A pattern similar to the co-location of shelf break and downdip end of rupture, albeit noisier, can be observed when interseismic locking is included (Figure 3). The resulting 48 data points are shown in Figure 3 A. This dataset includes all types of active margins, erosive shelf breaks but also depositional ones (sedimentary or volcanic, like Alaska or Kamchatka respectively); as well as different solutions for interseismic coupling at locations where it has been particularly difficult to constrain (Chilean Andes, Nankai, and North Honshu). In order to compare similar settings and locking patterns of high confidence, we further reduce the dataset to 21 sites by ignoring: interseismic constraints where good coseismic data is available (e.g. North Honshu); contradictory solutions for interseismic coupling (e.g. Chile); constructional shelf breaks set by the top of sedimentary foresets (Alaska, Ecuador-Colombia); or alternative solutions in sites where authors find equivalent patterns (Figure 3 B, details of the selection are in text S1 and Table S1 of the supplementary information). We also remove the Costa Rica subduction because of punctuated subduction erosion events that lead to transient changes in the accretionary prism geometry (Vannucchi et al., 2016). Finally, the Gorda subduction was also removed despite general overlap with Cascadia sites because of the amount of deformation accommodated by the very young oceanic crust itself as it subducts next to the Mendocino Triple Junction (Miller et al., 2001). The shelf breaks of the reduced set cluster around the locking depth with a mean distance of 4.7 km landward and 10<sup>th</sup> and 90<sup>th</sup> percentiles at -18 and 22 km. Coastlines, in contrast, are shifted landward with a mean distance of 43.1 km from the locking depth and 10<sup>th</sup> and 90<sup>th</sup> percentiles at 3.2 and 76.6 km (Figure 3 B, inset). A similar but less tight distribution is observed in the complete dataset (Figure 3 A, inset).

Despite the diversity in the structure and morphology of active margins (as documented in Noda, 2016), the edge of an erosive shelf is a markedly better predictor of the downdip end of locking than the coastline. Indeed, already recognizing that the coastline might not be a marker as reliable as they proposed, Ruff and Tichelaar (1996) noted that “continental shelf breaks [...] may have deeper physical significance [than the coastline]”. Additionally, in Cascadia, McNeill et al. (2000) identified that the outer arc high is co-located with the position of the locking depth on the megathrust and Booth-Rea



177 et al. (2008) noted that the seaward edge of the seismogenic transition lines up with the  
 178 shelf break. In the next section, we discuss which processes control the landscape of ac-  
 179 tive margins and underlie the observed co-location of downdip end of locking and shelf  
 180 break (Figure 2 and 3).

### 181 **3 A model for active margin shelves**

182 The edge of active margin shelves appears to be a reliable guide for the position  
 183 of the downdip end of locking on a megathrust (Figure 2 and 3). If information about  
 184 the coupling pattern of the megathrust is encoded in forearc morphology, it is crucial to  
 185 A) identify all first-order drivers of long-term deformation in order to isolate the signal  
 186 that is solely related to the subduction zone seismic cycle and B) understand how this  
 187 tectonic signal is encoded in the landscape morphology by erosive surface processes. The  
 188 surface elevation of the lithosphere  $z$  evolves as a function of the total rock uplift  $U_{\text{total}}$   
 189 and the surface erosion  $E$ :

$$\frac{\partial z}{\partial t} = U_{\text{total}} - E. \quad (1)$$

190 To explore the morphological evolution of an active margin following Eq. 1, we turn to  
 191 a simplified numerical model. We illustrate how coastlines get disconnected from tec-  
 192 tonic structures and evaluate how much of the long-term uplift signal is expressed in fore-  
 193 arc bathymetry when subjected to surface and seafloor shaping processes.

#### 194 **3.1 Sources of active deformation in an active forearc**

195 We summarize tectonic deformation at subduction margins as the sum of three main  
 196 components: 1) structural deformation from the growth of the forearc, 2) isostatic re-  
 197 sponse to denudation and sedimentation, and 3) long-term deformation driven by the  
 198 earthquake cycle (Figure 4). Together, they set the total rock uplift:

$$U_{\text{total}} = U_{\text{struct}} + U_{\text{iso}} + U_{\text{seismo}}. \quad (2)$$

199 Numerical models of coastal landscape evolution commonly use spatially uniform uplift  
 200 (Anderson et al., 1999; Snyder et al., 2002; Melnick, 2016), but here the non-uniform field  
 201 of uplift is key to understanding the reaction of the landscape and the stabilization of  
 202 the coastal domain. The relative magnitude of the three uplift components influences  
 203 the co-location of the locking depth and shelf break. In the absence of a mechanical model,

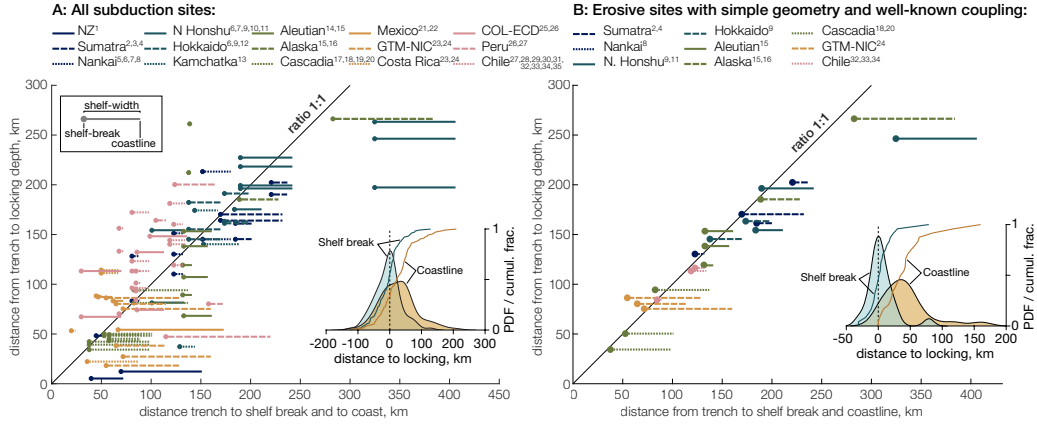


**Figure 3.** Position of the locking depth with respect to the shelf break and the coastline relative to the trench (inspired by Ruff and Tichelaar (1996)). Left: compilation of all surveyed sites (locations with multiple locking depth solutions are aligned vertically); right: compilation of sites with high confidence in locking depth position and erosive shelf breaks. The inset distributions show that shelf breaks are clustered around the locking depth while coastlines are shifted landward. For the indiscriminate compilation (left), the mean distance between shelf break and locking depth is -6.18 km (10<sup>th</sup>/90<sup>th</sup> percentiles at -61.5/40 km), and 25.17 km between coastline and locking depth (10<sup>th</sup>/90<sup>th</sup> percentiles of -43/93 km). For the high-confidence sites (right), the shelf breaks are tightly distributed at a mean distance of 4.7 km from the locking depth (10<sup>th</sup>/90<sup>th</sup> percentiles at -18/22 km) while coastlines are shifted and spread landward from it at a mean distance of 43.1 km (10<sup>th</sup>/90<sup>th</sup> percentiles at 3.2/76.6 km). Sources are 1: Wallace (2004), 2: Natawidjaja et al. (2007), 3: Chlieh et al. (2008), 4: Briggs et al. (2006), 5: Hyndman et al. (1995), 6: Mazzotti et al. (2000), 7: Loveless and Meade (2010), 8: Park et al. (2002), 9: Hashimoto et al. (2009), 10: Simons et al. (2011), 11: Lay et al. (2011), 12: Sawai et al. (2004), 13: Bürgmann (2005), 14: Cross and Freymueller (2007), 15: Johnson (1998), 16: Sykes et al. (1981), 17: Wang et al. (2003), 18: Burgette et al. (2009), 19: McCaffrey et al. (2007), 20: Schmalzle et al. (2014), 21: Radiguet et al. (2012), 22: Franco et al. (2012), 23: LaFemina et al. (2009), 24: Ye et al. (2013), 25: Kanamori and McNally (1982), 26: Nocquet et al. (2014), 27: Chlieh et al. (2011), 28: Metois et al. (2012), 29: Metois et al. (2013), 30: Metois et al. (2016), 31: Béjar-Pizarro et al. (2013), 32: Lay et al. (2014), 33: Yue et al. (2014), 34: (Li et al., 2016), 35: (Saillard et al., 2017).

204 we use arbitrary uplift profiles for structural and isostatic deformation, while the long-  
 205 term seismic deformation is obtained from a back slip model.

### 206 ***3.1.1 Structural deformation from the growth of the forearc.***

207 Noda (2016) proposed a classification of forearcs that is particularly relevant for  
 208 patterns of surface uplift or subsidence,  $U_{\text{struct}}$ , in the context of this study. Their struc-  
 209 tures can be organized along two axes: from extensional to compressional and from ero-  
 210 sional to accretionary (with respect to mass fluxes across the subduction channel, not  
 211 surface processes, Clift & Vannucchi, 2004). Most forearc systems are either extensional  
 212 and erosional *or* compressional and accretionary (Noda, 2016). The former are thinning  
 213 and subsiding and tend to develop deep forearc basins whereas the latter are thicken-  
 214 ing and uplifting and have smaller basins or widespread surface erosion (Noda, 2016).

215 The structural uplift field that represents deformation of the forearc under exten-  
 216 sion or compression is drawn arbitrarily to represent the two end-member configurations  
 217 under shortening (Figure 4 A) or extension (Figure 4 B). The structural deformation also  
 218 serves to stabilize the continental slope, representing thrusting in the accretionary wedge.

### 219 ***3.1.2 Isostatic response to denudation and sedimentation.***

220 Another important component of rock uplift is the isostatic response  $U_{\text{iso}}$  to sur-  
 221 face loading or unloading (e.g. Braun et al., 2014). Coastal ranges are eroding and rock  
 222 uplift should dominate landward while the offshore domain can be either erosive or aggra-  
 223 dational depending on the forearc type, which leads to either uplift or subsidence.

224 The isostatic response to denudation and sedimentation is modeled as an arbitrary  
 225 exponentially decaying uplift rate reaching zero at the trench in the case of solely pos-  
 226 itive rock uplift driven by denudation (Figure 4 A); to which a locus of subsidence cen-  
 227 tred around the forearc basin is added in the extensional case (Figure 4 B).

### 228 ***3.1.3 Long-term deformation driven by the earthquake cycle.***

229 Although standard models of subduction seismic cycles assume elastic interseismic  
 230 and coseismic deformation that perfectly balance each other (Savage, 1983), it is highly  
 231 plausible that repeated cycles of deformation lead to some fraction of non-recoverable

232 strain (e.g. King et al., 1988; Simpson, 2015). Permanent deformation can occur when-  
 233 ever stresses reach the plastic envelope of the upper plate forearc. This can occur dy-  
 234 namically at shallow depth during large seismic ruptures (e.g. Ma, 2012), or quasi-statically  
 235 near the base of the locked zone during interseismic loading (e.g. Vergne et al., 2001).  
 236 The associated anelastic deformation mechanisms could include various processes of brit-  
 237 tle rock fatigue, pressure-solution creep, or slip on pre-existing faults (Ashby & Sammis,  
 238 1990; Niemeijer & Spiers, 2002; Paterson & Wong, 2005; Brantut et al., 2013). In this  
 239 framework, the net sum of each coseismic and interseismic deformation represents an in-  
 240 crement of permanent deformation, which, integrated over many cycles, shapes a spe-  
 241 cific pattern of long-term uplift and subsidence  $U_{\text{seismo}}$  of the forearc.

242 Lacking detailed observational or physical constraints on the exact shape of per-  
 243 manent uplift and its relation to interseismic deformation, we postulate that the non-  
 244 recoverable uplift that builds up over many seismic cycles represents a fraction of the  
 245 vertical elastic displacement associated with the interseismic phase. This simplifying as-  
 246 sumption allows us to model the shape of permanent uplift with the standard back slip  
 247 approach (Savage, 1983; Kanda & Simons, 2010). Long-term interseismic rock uplift rates  
 248 is computed with a back slip model (Savage, 1983) using half-space elastic Green’s func-  
 249 tions (Okada, 1992) and assuming a fully locked region updip of the locking depth and  
 250 a transition zone downdip of it (see Bruhat & Segall, 2016, for details). The back slip  
 251 model assumes that surface deformation is due to elastic strain accumulation on and around  
 252 the plate interface and that it is equivalent to normal slip in the locked region. We com-  
 253 pute the distribution of interseismic surface uplift rates at an elevation of 0 m. Follow-  
 254 ing estimates by Le Pichon et al. (1998) and van Dinther et al. (2013), we use a fraction  
 255 (5%) of that deformation profile as a long-term field of uplift (Figure 5 A). It should be  
 256 noted that without quantitative constraints on erosional efficiency, the absolute value  
 257 of the uplift matters little while its spatial pattern is essential. The uplift hinge line pre-  
 258 dicted by the back slip model is generally located within 5 km of the locking depth but  
 259 can be displaced seaward with a gently dipping ( $< 10^\circ$ ) slab and in the absence of a tran-  
 260 sitional zone of partial locking (supplementary Figure S1).

### 261 **3.2 Sources of erosion**

262 The morphology of active margins is primarily controlled by the competition be-  
 263 tween 1) uplift, 2) erosion, and 3) sediment aggradation and transport (Bradley & Griggs,

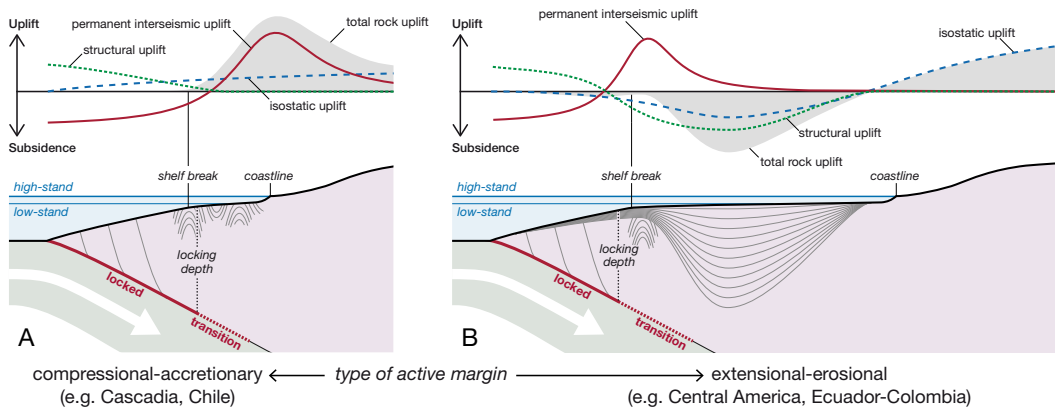


**Figure 4.** Conceptual model linking the morphology of active margins with the pattern of seismic locking on the megathrust. A: compressional-accretionary forearc end-member (sensu Noda, 2016). The combined patterns of permanent interseismic, isostatic, and structural uplift set the edge of the erosive shelf, landward of which rock uplift exposes bedrock to wave-base erosion (top). The shelf break lies close to the location of the downdip edge of locking, pinned by the locally strong gradient in interseismic uplift. The shelf grows landward from the edge by coastal retreat (bottom). B: Extensional-erosional end-member (erosion refers to subduction erosion here). Here, subsidence of the wedge overcomes permanent interseismic uplift (top) and the outer arc high acts as a sill for the forearc basin (bottom).

1976; Bouma et al., 1982; Anderson et al., 1999). We ignore subaerial erosion and sedimentation processes to focus on wave-base erosion. We adopt the phenomenological model of Anderson et al. (1999), which expends ocean wave energy on the shallow seafloor for wave-base erosion, leaving the remainder (if any) for sea-cliff erosion. First, offshore wave energy  $P_0$  is expended and transformed into vertical erosion ( $\partial z/\partial t$ ) depending on water depth  $h$  as the waves move closer to the shore:

$$\frac{\partial z}{\partial t} = \beta_z P_0 \exp\left(-\frac{4h}{h_{wb}}\right), \quad (3)$$

where  $\beta_z$  is an incision coefficient and  $h_{wb}$  is the depth of wave base. The remainder of the offshore energy is then transformed into a rate of cliff retreat  $\partial x/\partial t$ :

$$\frac{\partial x}{\partial t} = \beta_x \left[ P_0 - \int_{shelf} P_0 \exp\left(-\frac{4h}{h_{wb}}\right) dx \right]. \quad (4)$$

The erosion component is driven by the sea level curve of Spratt and Lisiecki (2016) looped over 2 Myr for a naturally noisy eustatic signal. Wave energy is assumed constant through time. This is the best available code to investigate the first-order morphodynamics controlling eroding margins and it produces realistic looking topography. However, it can not be used to quantitatively invert a topographic profile and reconstruct either a history of uplift or sea-level as the two key coefficients  $\beta_x$  and  $\beta_z$  cannot be calibrated with more precision than a visual fit with non-unique parametrization allows.

### 3.3 Results

The transition from subsidence (seaward) to uplift (landward), hereafter referred to as hinge line, acts as an anchor point for seafloor topography, which constantly evolves in response to wave base erosion. As illustrated below, the localization of this hinge-line above or near the locking depth would result from the permanent, interseismic-like component of total rock uplift (Figure 5).

The effect of a localized peak of uplift driven by interseismic deformation is critical in all types of forearc geometries (see Noda, 2016). For the compressional-accretionary end-member (Figure 4 A) the associated uplift peak marks the beginning of the domain where rocks are advected into the zone of wave-base erosion (and subaerial erosion landward of the coast). For the extensional-erosional end-member, the interseismic uplift peak may not overcome structural and isostatic subsidence driven by extension and sedimentation but the peak can create a sill for the forearc basin by reducing subsidence locally

292 (Figure 4 B). In both cases, the resulting structure would be compatible with the outer  
 293 arc-high (Seely & Dickinson, 1977; McNeill et al., 2000; Booth-Rea et al., 2008) and it  
 294 would anchor a continental shelf that can grow landward by coastal erosion. The Mat-  
 295 lab source code of the model is available in the supplementary material with a list of pa-  
 296 rameters to reproduce the simulations presented here along with three videos of the runs  
 297 shown in Figure 5.

### 298 **Wide erosive shelves**

299 The morphology of wide, largely erosive, shelves of the Cascadia margin type (Fig-  
 300 ure 1) is characterized by a shelf break (outer arc high) above the locking depth and a  
 301 wide platform beveled by wave base erosion that displaced the coast landward (Figure 5  
 302 A). When wave energy is strong enough, and/or rock strength or uplift rate weak enough,  
 303 the shelf can extend well beyond the peak of interseismic uplift. In this situation, the  
 304 interseismic deformation signal recorded by onshore geodetic stations or surveys would  
 305 reflect increasing interseismic uplift rates shoreward, as is the case in Cascadia (Burgette  
 306 et al., 2009). Notably, landward of the uplift maximum, the erosion potential of wave  
 307 energy enables an increasingly larger footprint as waves face slower uplift rates.

### 308 **Wide subsiding shelves**

309 In extensional-erosional active margins (subduction erosion) of the type found in  
 310 Central America (Figure 1, Noda, 2016), the coastline is further removed from the shelf  
 311 break by a subsiding basin. The model run of Figure 5 B illustrates this situation. For  
 312 the incoming high-stand waves, the subsiding domain would have a relatively small en-  
 313 ergy cost limited to the transport of sediment on the shelf and wave-energy can be con-  
 314 served over a large distance to erode the coast farther. The magnitude of interseismic  
 315 deformation signals that could be picked up by onshore geodetic monuments is accord-  
 316 ingly severely reduced. Note that we are not modeling sedimentary dynamics here and  
 317 that there is no energy expenditure at all over the subsiding basin.

### 318 **Narrow erosive shelves**

319 Narrow shelves, like those found in Northern Chile, can principally result from two  
 320 characteristics: a strong lithology preventing the erosion of a wide platform, or fast up-

321 lift rates feeding a large volume of rock in the wave-base erosion domain. As long as long-  
 322 term interseismic deformation dominates the uplift pattern, the co-location of shelf break  
 323 and locking depth should be preserved and the coastline would be closely aligned. In con-  
 324 trast, if the uplift pattern is dominated by non-interseismic factors, the co-location is lost.  
 325 As illustrated in Figure 5 C, if a strong isostatic uplift rate dominates, the shelf break  
 326 is shifted seaward significantly.

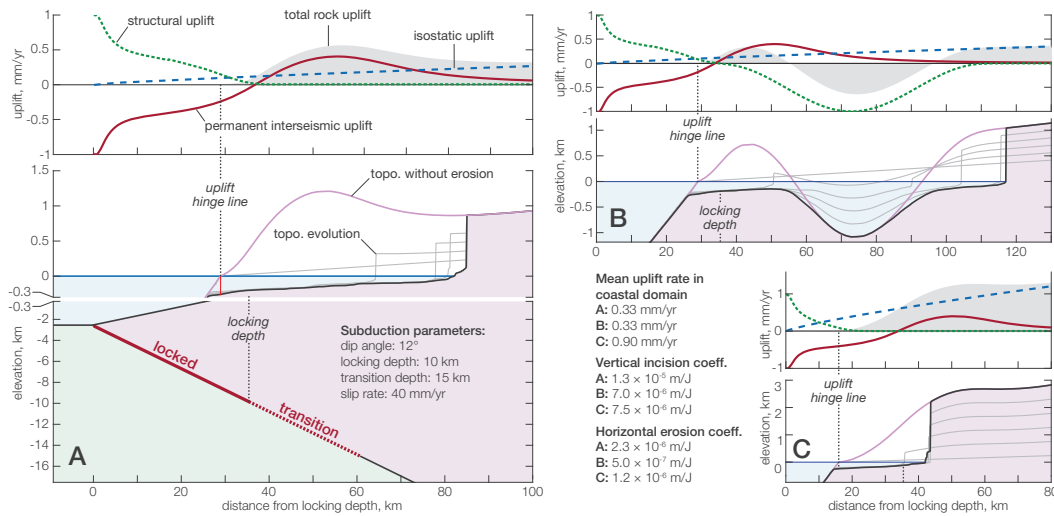


**Figure 5.** Numerical model illustrating the relationship between coastal morphology and subduction locking patterns. Wave-base and cliff erosion following Anderson et al. (1999) are the only surface processes (no sedimentation, no subaerial erosion). Interseismic deformation is derived from the back slip model (adapted from Savage, 1983; Okada, 1992) of a locked fault. A: reference case with a wide shelf reflecting local uplift rates dominated by interseismic signature and relatively high rock erodibility. The vertical scale is exaggerated from -300 to 1000 m. B: subsidence of a forearc basin further separates outer arc high and coast. C: uplift rate is dominated by continental isostatic uplift and relatively low rock erodibility. In this case, the uplift hinge-line is significantly offset from the position of the locking depth by the fast continental uplift. All models are run with the same subduction parameters and offshore wave energy. Videos for each of these runs are available in the supplementary material.



## 4 Perspectives and conclusion

### 4.1 Source of variability and commonalities in the compilation

Unlike the structural and isostatic components of uplift, the permanent seismic cycle component varies at short wavelength and is similar across subduction zones. It provides a straightforward connection between seismic cycle deformation and the morphology of the coastal domain. It is therefore a plausible candidate to explain the co-location of the locking depth and the shelf break. Further investigating this idea will first require a mechanistic model for the spatial pattern of long-term permanent uplift. Interestingly, a growing body of observations suggests that it should resemble elastic deformation associated with the interseismic phase of the seismic cycle. For example, Allmendinger et al. (2009) noted that “at a regional scale within continents, interseismic deformation is mostly nearly similar to regional late Cenozoic tectonic deformation”. Work from Loveless and Allmendinger (2005) showed that the extensional strain field predicted by elastic interseismic deformation co-locates with regions of normal faulting in the Coastal Cordillera of Chile. Stevens and Avouac (2015) noted that the uplift pattern predicted by coupling on the Main Himalayan Thrust mimics the topography of the mountain range. Coastal uplift above subduction zones has also been partly attributed to interseismic deformation based on the pattern of deformed terraces in Cascadia (Kelsey & Bockheim, 1994; Personius, 1995), on the co-location of peninsulas and shallow locking depth in the Andes (Saillard et al., 2017), and on the growth of the Japanese coastal mountains (Yoshikawa, 1968; Yoshikawa et al., 1981; Le Pichon et al., 1998).

The deformation derived from permanent interseismic deformation can be reasonably expected to be largely similar from one locked megathrust to another, as subduction earthquake cycles share many similarities. By contrast, the pattern of isostatic uplift or subsidence is expected to vary according to the regimes of denudation and deposition but to retain an overall similarity with more uplift landward and less (or more negative) uplift seaward. In this framework, the large structural and morphological diversity of forearc basins mainly stems from the forearc deformation set by its mass balance (erosional vs. accretionary, Noda, 2016).

The scatter around the position of the locking depth in Figure 2 and 3 may result from a combination of factors, chiefly among them uncertainties in the inversion of interseismic coupling and coseismic ruptures, and differences between the pattern of anelas-

359 tic versus elastic interseismic deformation. The relative magnitudes of the three uplift  
 360 components can alter the relationship between locking depth and shelf break. This is il-  
 361 lustrated by the model run of Figure 5 C where isostatic deformation dominates the to-  
 362 tal uplift.

## 363 4.2 Critical taper and other modes of deformation

364 Critical taper theory (Dahlen, 1984) is essential to explain the full deformation pat-  
 365 tern of active margins (here named *structural uplift*). It could also provide an alterna-  
 366 tive explanation for the pattern of deformation that we ascribe to permanent interseis-  
 367 mic deformation. The deformation pattern of a critical wedge changes in response to vari-  
 368 ations in basal friction such that a vertical shear zone marking the onset of landward up-  
 369 lift could localize above the locking depth (Fuller et al., 2006; Cubas et al., 2013). How-  
 370 ever, for this hinge line to develop, the wedge has to be critical, which is a condition only  
 371 met in parts of a few subduction zones (Cubas et al., 2013; Rousset et al., 2016; Koulali  
 372 et al., 2018). Given the limited occurrence of critically tapered subduction zones glob-  
 373 ally, we find that anelastic interseismic deformation provides a more plausible explana-  
 374 tion for the global signal of locking depths revealed by coastal geomorphology (Figure 3).  
 375 Nevertheless, if the outer-arc high uplift is not caused by permanent interseismic defor-  
 376 mation as we argue here, it is likely that its connection to the regime of coupling on the  
 377 megathrust could be elucidated by looking at patterns of internal deformation of crit-  
 378 ical wedges.

379 Rare deep earthquakes in the partially locked zone C *sensu* Lay et al. (2012), i.e.  
 380 deeper than the locking depth, have been proposed to drive coastal uplift in the Cen-  
 381 tral Andes by Melnick (2016). In this hypothesis, the coseismic uplift of earthquakes in  
 382 the shallower locked zones A and B would be compensated by subsidence during the post-  
 383 and interseismic periods, unlike their rarer and deeper zone C counterparts. It is unclear  
 384 why this deep coseismic component alone is not compensated and why it would be the  
 385 driver of permanent seismogenic deformation at subduction margins while much greater  
 386 seismogenic slip occurs on fully locked zones A and B (Lay et al., 2012).

387 Our modeling focuses on the interaction between uplift and wave-base erosion that  
 388 shapes the continental shelf. We do not address the subsiding parts of the margin. How-  
 389 ever, observations of deformation and sedimentation in zones of interseismic subsidence

390 support our assumption and complements our work on the erosive part of the system.  
 391 The locked domain of megathrusts has been observed to be often overlain by large fore-  
 392 arc basins on deep sea terraces seaward of the shelf (Sugiyama, 1994; Song & Simons,  
 393 2003; Wells et al., 2003). These deep subsiding forearc basins have been attributed to  
 394 subduction erosion (Wells et al., 2003), and to critical taper deformation of the inner wedge  
 395 (Fuller et al., 2006; Wang & Hu, 2006; Cubas et al., 2013). If these forearc basins are  
 396 indeed the depositional counterparts of erosive shelves and are driven by long-term in-  
 397 terseismic deformation, then their stratigraphy could inform the temporal stability of  
 398 the locking pattern in a manner that erosion on the shelf cannot.

### 399 4.3 A bridge between seismic and landscape timescales

400 Geodetic measurements of interseismic coupling or coseismic ruptures reflect at most  
 401 a few centuries of geological history. Meanwhile, the landscape records the effect of tec-  
 402 tonics and surface processes over hundreds to thousands of individual seismic cycles span-  
 403 ning 100's of kyrs (e.g. Valensise & Ward, 1991; Willett et al., 1993; Lavé & Avouac, 2001;  
 404 Avouac, 2003). Hence, if the position of the locking depth is stable — as expected from  
 405 a fault with a characteristic earthquake cycle, where the region locked during the inter-  
 406 seismic period exactly delimits the extent of future earthquakes — the same domains are  
 407 in net rock subsidence or rock uplift 100% of the time and the shelf break should be a  
 408 sharp morphological marker (like in Cascadia potentially, Figure 6).

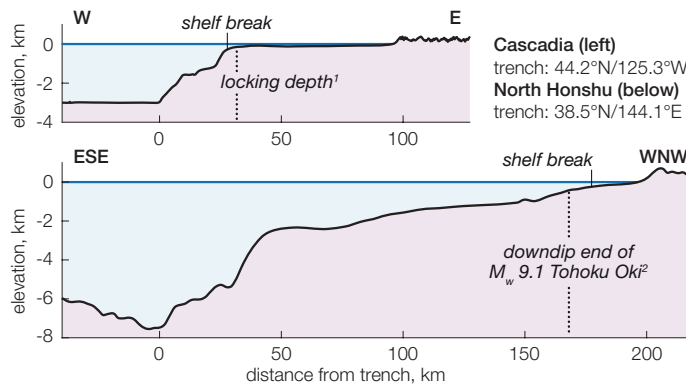


**Figure 6.** Profiles across the Cascadia and North Honshu margins. In Cascadia, the shelf break is a sharp and salient feature while in North Honshu the shelf break is lost in the upper continental slope. Both figures share the same scale. 1: Burgette et al. (2009); 2: Lay et al. (2011)

409 While the assumption of a characteristic earthquake cycle is common, interseismic  
410 coupling might also plausibly vary over several seismic cycles, leading to a more poorly  
411 defined shelf break (such as observed in Japan, Figure 6) because the transition from sub-  
412 siding all of the time to uplifting all of the time would not be well defined spatially . Ad-  
413 ditionally, within the interseismic period itself, there is increasing evidence that coupling  
414 distribution could be time-dependent. The downdip end of coupling could migrate up-  
415 dip during the interseismic period, resulting in variable degrees of possible mismatch be-  
416 tween coseismic reconstructions and current interseismic measurements (Thatcher, 1984;  
417 Schmalzle et al., 2014; Nishimura, 2014; Jiang & Lapusta, 2016; Wang & Tréhu, 2016;  
418 Bruhat & Segall, 2017).

419 Beyond temporal variations, the pattern of long-term uplift depends as much on  
420 the spatial distribution of interseismic deformation as on that of coseismic displacement.  
421 Coseismic deformation can also locally overcome interseismic deformation as in Suma-  
422 tra (Sieh et al., 2008; Philibosian et al., 2014), or their respective spatial distributions  
423 could differ Penserini et al. (2017). The model proposed here opens the exploration of  
424 long-term stability or transience of interseismic locking patterns.

#### 425 **4.4 Conclusion**

426 We observe that the edge of a subduction margin shelf is a markedly better indi-  
427 cator of the downdip end of locking on the megathrust than the coastline. We propose  
428 that this co-location directly results from the pattern of permanent interseismic defor-  
429 mation that drives a relative peak in uplift rate just landward of the downdip edge of  
430 locking. We show that a model combining permanent interseismic deformation with wave-  
431 base erosion reproduces the first order alignment of shelf breaks above the seismic lock-  
432 ing depths of subduction megathrusts, as observed in a global survey. We present a first-  
433 order relationship between active margin morphology and seismogenic patterns at depth.  
434 This proposition calls for future validation in the form of mechanical modeling and field  
435 observations. The morphological expression of the seismogenic characteristics of a megath-  
436 rust is particularly valuable where shelves are wide and onshore geodetic surveys accord-  
437 ingly limited. The submarine landscape of an active margin integrates repeated seismic  
438 cycles and bridges seismic timescales (100's of yrs) with those of landscape building (100's  
439 of kyrs). As a result, the stability or transience of seismic coupling would be recorded  
440 in the morphology of the shelf break itself.

## Acknowledgments

We thank Jean-Philippe Avouac, Emily Brodsky, Nadaya Cubas, Cécile Lasserre, Thorne Lay, Marianne Métois, and Baptiste Rousset for stimulating discussions. We acknowledge two anonymous reviewers for their comments. Malatesta was supported by a Post.Doc Mobility fellowship of the Swiss National Science Foundation (P2SKP2\_168328). Bruhat has received funding from the People Programme (Marie Curie Actions) of the European Unions Seventh Framework Programme (FP7/2007-2013) under REA grant agreement n. PCOFUND-GA-2013-609102, through the PRESTIGE programme coordinated by Campus France. Olive was supported by an Emergence(s) – Ville de Paris grant. All information supporting this contribution is present in the main manuscript or the supplementary material. The MATLAB code for the numerical model as well as the compilation of locations are available in the Supplementary Information.

## References

- Aki, K. (1967). Scaling law of seismic spectrum. *Journal of Geophysical Research: Planets*, *72*(4), 1217–1231.
- Allmendinger, R. W., Loveless, J. P., Pritchard, M. E., & Meade, B. (2009, November). From decades to epochs: Spanning the gap between geodesy and structural geology of active mountain belts. *Journal Of Structural Geology*, *31*(11), 1409–1422.
- Anderson, R. S., Densmore, A. L., & Ellis, M. A. (1999, March). The generation and degradation of marine terraces. *Basin Research*, *11*(1), 7–19.
- Ashby, M. F., & Sammis, C. G. (1990). The Damage Mechanics of Brittle Solids in Compression. *Pure and Applied Geophysics*, *133*(3), 489–521.
- Avouac, J.-P. (2003). Mountain building, erosion, and the seismic cycle in the Nepal Himalaya. *Advances in Geophysics*.
- Béjar-Pizarro, M., Socquet, A., Armijo, R., Carrizo, D., Genrich, J., & Simons, M. (2013, April). Andean structural control on interseismic coupling in the North Chile subduction zone. *Nature Geoscience*, *6*(6), 462–467.
- Booth-Rea, G., Klaeschen, D., Grevemeyer, I., & Reston, T. (2008, July). Heterogeneous deformation in the Cascadia convergent margin and its relation to thermal gradient (Washington, NW USA). *Tectonics*, *27*(4), 1–15.
- Bouma, A. H., Berryhill, H. L., Brenner, R. L., & Knebel, H. J. (1982, January).

- 473 Continental Shelf and Epicontinental Seaways. *Sandstone Depositional Envi-*  
 474 *ronments*, 31, 0.
- 475 Bradley, W. C., & Griggs, G. B. (1976, March). Form, genesis, and deformation of  
 476 central California wave-cut platforms. *Geological Society of America Bulletin*,  
 477 87(3), 433–449.
- 478 Brantut, N., Heap, M. J., Meredith, P. G., & Baud, P. (2013, July). Time-  
 479 dependent cracking and brittle creep in crustal rocks: A review. *Journal*  
 480 *Of Structural Geology*, 52(C), 17–43.
- 481 Braun, J., Simon-Labric, T., Murray, K. E., & Reiners, P. W. (2014, June). Topo-  
 482 graphic relief driven by variations in surface rock density. *Nature Geoscience*.
- 483 Briggs, R. W., Sieh, K., Meltzner, A. J., Natawidjaja, D. H., Galetzka, J., Suwar-  
 484 gadi, B. W., . . . Bock, Y. (2006). Deformation and slip along the Sunda  
 485 Megathrust in the great 2005 Nias-Simeulue earthquake. *Science*, 311(5769),  
 486 1897–1901.
- 487 Brooks, B. A., Bevis, M., Whipple, K., Arrowsmith, J. R., Foster, J., Zapata, T., . . .  
 488 Smalley, R. J. (2011, May). Orogenic-wedge deformation and potential for  
 489 great earthquakes in the central Andean backarc. *Nature Geoscience*, 4(6),  
 490 380–383.
- 491 Bruhat, L., & Segall, P. (2016, November). Coupling on the northern Cascadia sub-  
 492 duction zone from geodetic measurements and physics-based models. *Journal*  
 493 *of Geophysical Research*, 121(11), 8297–8314.
- 494 Bruhat, L., & Segall, P. (2017, July). Deformation rates in northern Cascadia consis-  
 495 tent with slow updip propagation of deep interseismic creep. *Geophysical Jour-*  
 496 *nal International*, 211(1), 427–449.
- 497 Burgette, R. J., Weldon II, R. J., & Schmidt, D. A. (2009, January). Interseis-  
 498 mic uplift rates for western Oregon and along-strike variation in locking on  
 499 the Cascadia subduction zone. *Journal of Geophysical Research*, 114(B1),  
 500 TC3009–24.
- 501 Bürgmann, R. (2005). Interseismic coupling and asperity distribution along the  
 502 Kamchatka subduction zone. *Journal of Geophysical Research*, 110(B7), 1675–  
 503 17.
- 504 Bürgmann, R., & Chadwell, D. (2014, May). Seafloor Geodesy. *Annual Review Of*  
 505 *Earth And Planetary Sciences*, 42(1), 509–534.

- 506 Chlieh, M., Avouac, J.-P., Sieh, K., Natawidjaja, D. H., & Galetzka, J. (2008, May).  
 507 Heterogeneous coupling of the Sumatran megathrust constrained by geodetic  
 508 and paleogeodetic measurements. *Journal of Geophysical Research-Solid Earth*  
 509 *and Planets*, *113*(B5), 2018–31.
- 510 Chlieh, M., Perfettini, H., Tavera, H., Avouac, J.-P., Remy, D., Nocquet, J.-M., ...  
 511 Bonvalot, S. (2011, December). Interseismic coupling and seismic potential  
 512 along the Central Andes subduction zone. *Journal of Geophysical Research*,  
 513 *116*(B12), B10404–21.
- 514 Clift, P., & Vannucchi, P. (2004). Controls on tectonic accretion versus erosion in  
 515 subduction zones: Implications for the origin and recycling of the continental  
 516 crust. *Reviews of Geophysics and Space Physics*, *42*(2), 1–31.
- 517 Cramer, F. (2018). Geodynamic diagnostics, scientific visualisation and StagLab  
 518 3.0. *Geoscientific Model Development*, *11*(6), 2541–2562.
- 519 Cross, R. S., & Freymueller, J. T. (2007, March). Plate coupling variation and block  
 520 translation in the Andreanof segment of the Aleutian arc determined by sub-  
 521 duction zone modeling using GPS data. *Geophysical Research Letters*, *34*(6),  
 522 1653–5.
- 523 Cubas, N., Avouac, J.-P., Souloumiac, P., & Leroy, Y. (2013, November). Megath-  
 524 rust friction determined from mechanical analysis of the forearc in the Maule  
 525 earthquake area. *Earth and Planetary Science Letters*, *381*(C), 92–103.
- 526 Dahlen, F. A. (1984). Noncohesive Critical Coulomb Wedges - an Exact Solution.  
 527 *Journal of Geophysical Research*, *89*, 125–133.
- 528 Dragert, H., Wang, K. L., & James, T. S. (2001). A silent slip event on the deeper  
 529 Cascadia subduction interface. *Science*, *292*(5521), 1525–1528.
- 530 Franco, A., Lasserre, C., Lyon-Caen, H., Kostoglodov, V., Molina, E., Guzman-  
 531 Speziale, M., ... Manea, V. C. (2012, April). Fault kinematics in northern  
 532 Central America and coupling along the subduction interface of the Cocos  
 533 Plate, from GPS data in Chiapas (Mexico), Guatemala and El Salvador. *Geo-*  
 534 *physical Journal International*, *189*(3), 1223–1236.
- 535 Fuller, C., Willett, S. D., & Brandon, M. T. (2006). Formation of forearc basins and  
 536 their influence on subduction zone earthquakes. *Geology*, *34*(2), 65–68.
- 537 Hashimoto, C., Noda, A., Sagiya, T., & Matsu'ura, M. (2009, January). Interplate  
 538 seismogenic zones along the Kuril-Japan trench inferred from GPS data inver-

- 539 sion. *Nature Geoscience*, 2(2), 141–144.
- 540 Hyndman, R. D., Wang, K., & Yamano, M. (1995, August). Thermal constraints on  
541 the seismogenic portion of the southwestern Japan subduction thrust. *Journal*  
542 *of Geophysical Research: Planets*, 100(B8), 15373–15392.
- 543 James, T. S., Gowan, E. J., Wada, I., & Wang, K. (2009, April). Viscosity of the  
544 asthenosphere from glacial isostatic adjustment and subduction dynamics at  
545 the northern Cascadia subduction zone, British Columbia, Canada. *Journal of*  
546 *Geophysical Research-Solid Earth and Planets*, 114(B4), 536–13.
- 547 Jiang, J., & Lapusta, N. (2016, June). Deeper penetration of large earthquakes on  
548 seismically quiescent faults. *Science*, 352(6291), 1293–1297.
- 549 Johnson, J. M. (1998). Heterogeneous Coupling Along Alaska-Aleutians as Inferred  
550 From Tsunami, Seismic, and Geodetic Inversions. In *Tsunamigenic earthquakes*  
551 *and their consequences* (pp. 1–116). Elsevier.
- 552 Kanamori, H., & McNally, K. C. (1982, August). Variable rupture mode of the sub-  
553 duction zone along the Ecuador-Colombia coast. *Bulletin of the Seismological*  
554 *Society of America*, 72(4), 1241–1253.
- 555 Kanda, R. V. S., & Simons, M. (2010). An elastic plate model for interseismic  
556 deformation in subduction zones. *Journal of Geophysical Research: Planets*,  
557 115(B3), 2328.
- 558 Kelsey, H. M., & Bockheim, J. G. (1994, June). Coastal landscape evolution as a  
559 function of eustasy and surface uplift rate, Cascadia margin, southern Oregon.  
560 *Geological Society of America Bulletin*, 106(6), 840–854.
- 561 King, G. C. P., Stein, R. S., & Rundle, J. B. (1988). The Growth of Geological  
562 Structures by Repeated Earthquakes .1. Conceptual-Framework. *Journal of*  
563 *Geophysical Research*, 93, 13307–13318.
- 564 Konca, A. O., Avouac, J.-P., Sladen, A., Meltzner, A. J., Sieh, K., Fang, P., ...  
565 Helmberger, D. (2008, December). Partial rupture of a locked patch of the  
566 Sumatra megathrust during the 2007 earthquake sequence. *Nature*, 456(7222),  
567 631–635.
- 568 Koulali, A., McClusky, S., Cummins, P., & Tregoning, P. (2018, June). Wedge ge-  
569 ometry, frictional properties and interseismic coupling of the Java megathrust.  
570 *Tectonophysics*, 734-735, 89–95.
- 571 LaFemina, P., Dixon, T. H., Govers, R., Norabuena, E., Turner, H., Saballos, A.,



- 572 ... Strauch, W. (2009, May). Fore-arc motion and Cocos Ridge collision in  
573 Central America. *Geochemistry Geophysics Geosystems*, *10*(5), n/a–n/a.
- 574 Larsen, S., & Reilinger, R. (1992, June). Global positioning system measurements of  
575 strain accumulation across the Imperial Valley, California: 1986–1989. *Journal*  
576 *of Geophysical Research: Planets*, *97*(B6), 8865–8876.
- 577 Lavé, J., & Avouac, J.-P. (2001, January). Fluvial incision and tectonic uplift across  
578 the Himalayas of central Nepal. *Journal of Geophysical Research*, *106*(B11),  
579 26561–26,591.
- 580 Lay, T., Ammon, C. J., Kanamori, H., Xue, L., & Kim, M. J. (2011, September).  
581 Possible large near-trench slip during the 2011  $M_w$ 9.0 off the Pacific coast of  
582 Tohoku Earthquake. *Earth, Planets and Space*, *63*(7), 687–692.
- 583 Lay, T., Kanamori, H., Ammon, C. J., Koper, K. D., Hutko, A. R., Ye, L., ... Rush-  
584 ing, T. M. (2012, April). Depth-varying rupture properties of subduction zone  
585 megathrust faults. *Journal of Geophysical Research*, *117*(B4), n/a–n/a.
- 586 Lay, T., Yue, H., Brodsky, E. E., & An, C. (2014, June). The 1 April 2014 Iquique,  
587 Chile,  $M_w$ 8.1 earthquake rupture sequence. *Geophysical Research Letters*,  
588 *41*(11), 3818–3825.
- 589 Le Pichon, X., Mazzotti, S., Henry, P., & Hashimoto, M. (1998, August). Deforma-  
590 tion of the Japanese Islands and seismic coupling: an interpretation based on  
591 GSI permanent GPS observations. *Geophysical Journal International*, *134*(2),  
592 501–514.
- 593 Li, L., Lay, T., Cheung, K. F., & Ye, L. (2016, May). Joint modeling of teleseismic  
594 and tsunami wave observations to constrain the 16 September 2015 Illapel,  
595 Chile,  $M_w$ 8.3 earthquake rupture process. *Geophysical Research Letters*, *43*(9),  
596 4303–4312.
- 597 Loveless, J. P., & Allmendiger, R. W. (2005). Implications of elastic dislocation  
598 modeling on permanent deformation in the Northern Chilean forearc. In *Inter-*  
599 *national symposium on andean geodynamics* (pp. 454–457). Barcelona.
- 600 Loveless, J. P., & Meade, B. J. (2010, February). Geodetic imaging of plate mo-  
601 tions, slip rates, and partitioning of deformation in Japan. *Journal of Geophys-*  
602 *ical Research*, *115*(B2), L11303–35.
- 603 Ma, S. (2012, June). A self-consistent mechanism for slow dynamic deformation and  
604 tsunami generation for earthquakes in the shallow subduction zone. *Geophysi-*

- 605 *cal Research Letters*, 39(11), n/a–n/a.
- 606 Mai, P. M., & Beroza, G. C. (2000, June). Source Scaling Properties from Finite-  
607 Fault-Rupture Models. *Bulletin of the Seismological Society of America*, 90(3),  
608 604–615.
- 609 Mazzotti, S., Le Pichon, X., Henry, P., & Miyazaki, S.-I. (2000, June). Full inter-  
610 seismic locking of the Nankai and Japan-west Kurile subduction zones: An  
611 analysis of uniform elastic strain accumulation in Japan constrained by perma-  
612 nent GPS. *Journal of Geophysical Research*, 105(B6), 13159–13177.
- 613 McCaffrey, R., Qamar, A. I., King, R. W., Wells, R., Khazaradze, G., Williams,  
614 C. A., . . . Zwick, P. C. (2007, June). Fault locking, block rotation and crustal  
615 deformation in the Pacific Northwest. *Geophysical Journal International*,  
616 169(3), 1315–1340.
- 617 McNeill, L. C., Goldfinger, C., Kulm, L. D., & Yeats, R. S. (2000, August). Tec-  
618 tonics of the Neogene Cascadia forearc basin: Investigations of a deformed  
619 late Miocene unconformity. *Geological Society of America Bulletin*, 112(8),  
620 1209–1224.
- 621 Melnick, D. (2016, March). Rise of the central Andean coast by earthquakes strad-  
622 dling the Moho. *Nature Geoscience*, 9(5), 401–407.
- 623 Metois, M., Socquet, A., & Vigny, C. (2012, March). Interseismic coupling, segmen-  
624 tation and mechanical behavior of the central Chile subduction zone. *Journal*  
625 *of Geophysical Research*, 117(B3), 40–16.
- 626 Metois, M., Vigny, C., & Socquet, A. (2016, April). Interseismic Coupling, Megath-  
627 rust Earthquakes and Seismic Swarms Along the Chilean Subduction Zone  
628 (38°–18°S). *Pure and Applied Geophysics*, 173(5), 1431–1449.
- 629 Metois, M., Vigny, C., Socquet, A., Delorme, A., Morvan, S., Ortega, I., & Valderas-  
630 Bermejo, C. M. (2013, November). GPS-derived interseismic coupling on the  
631 subduction and seismic hazards in the Atacama region, Chile. *Geophysical*  
632 *Journal International*, 196(2), 644–655.
- 633 Miller, M. M., Johnson, D. J., Rubin, C. M., Dragert, H., Wang, K., Qamar, A., &  
634 Goldfinger, C. (2001, April). GPS-determination of along-strike variation in  
635 Cascadia margin kinematics: Implications for relative plate motion, subduction  
636 zone coupling, and permanent deformation. *Tectonics*, 20(2), 161–176.
- 637 Natawidjaja, D. H., Sieh, K., Galetzka, J., Suwargadi, B. W., Cheng, H., Edwards,

- 638 R. L., & Chlieh, M. (2007, February). Interseismic deformation above the  
 639 Sunda Megathrust recorded in coral microatolls of the Mentawai islands, West  
 640 Sumatra. *Journal of Geophysical Research-Solid Earth and Planets*, *112*(B2),  
 641 1897–27.
- 642 Niemeijer, A. R., & Spiers, C. J. (2002, January). Compaction creep of quartz-  
 643 muscovite mixtures at 500°C: Preliminary results on the influence of muscovite  
 644 on pressure solution. *Geological Society, London, Special Publications*, *200*(1),  
 645 61–71.
- 646 Nishimura, T. (2014, June). Pre-, Co-, and Post-Seismic Deformation of the 2011  
 647 Tohoku-Oki Earthquake and its Implication to a Paradox in Short-Term and  
 648 Long-Term Deformation. *Journal of Disaster Research*, *9*(3), 294–302.
- 649 Nishimura, T., Hirasawa, T., Miyazaki, S., Sagiya, T., Tada, T., Miura, S., &  
 650 Tanaka, K. (2004, May). Temporal change of interplate coupling in north-  
 651 eastern Japan during 1995–2002 estimated from continuous GPS observations.  
 652 *Geophysical Journal International*, *157*(2), 901–916.
- 653 Nocquet, J.-M., Villegas-Lanza, J. C., Chlieh, M., Mothes, P. A., Rolandone, F.,  
 654 Jarrin, P., . . . Yepes, H. (2014, March). Motion of continental slivers and  
 655 creeping subduction in the northern Andes. *Nature Geoscience*, *7*(4), 287–  
 656 291.
- 657 Noda, A. (2016, April). Forearc basins: Types, geometries, and relationships to sub-  
 658 duction zone dynamics. *Geological Society of America Bulletin*, *128*(5-6), 879–  
 659 895.
- 660 Obara, K. (2002). Nonvolcanic deep tremor associated with subduction in southwest  
 661 Japan. *Science*, *296*(5573), 1679–1681.
- 662 Okada, Y. (1992, April). Internal deformation due to shear and tensile faults in a  
 663 half-space. *Bulletin of the Seismological Society of America*, *82*(2), 1018–1040.
- 664 Park, J.-O., Tsuru, T., Kodaira, S., Cummins, P. R., & Kaneda, Y. (2002, Au-  
 665 gust). Splay Fault Branching Along the Nankai Subduction Zone. *Science*,  
 666 *297*(5584), 1157–1160.
- 667 Paterson, M. S., & Wong, T.-f. (2005). *Experimental Rock Deformation - The Brittle*  
 668 *Field*. Springer Science & Business Media.
- 669 Penserini, B. D., Roering, J. J., & Streig, A. (2017, April). A morphologic proxy  
 670 for debris flow erosion with application to the earthquake deformation cycle,

- 671 Cascadia Subduction Zone, USA. *Geomorphology*, 282(C), 150–161.
- 672 Personius, S. F. (1995). Late Quaternary stream incision and uplift in the forearc  
673 of the Cascadia subduction zone, western Oregon - Personius - 1995 - Jour-  
674 nal of Geophysical Research: Solid Earth - Wiley Online Library. *Journal of*  
675 *Geophysical Research*.
- 676 Philibosian, B., Sieh, K., Avouac, J.-P., Natawidjaja, D. H., Chiang, H.-W., Wu,  
677 C.-C., ... Suwargadi, B. W. (2014, September). Rupture and variable coupling  
678 behavior of the Mentawai segment of the Sunda megathrust during the super-  
679 cycle culmination of 1797 to 1833. *Journal of Geophysical Research*, 119(9),  
680 7258–7287.
- 681 Radiguet, M., Cotton, F., Vergnolle, M., Campillo, M., Walpersdorf, A., Cotte, N.,  
682 & Kostoglodov, V. (2012, April). Slow slip events and strain accumulation  
683 in the Guerrero gap, Mexico. *Journal of Geophysical Research*, 117(B4),  
684 n/a–n/a.
- 685 Rousset, B., Lasserre, C., Cubas, N., Graham, S., Radiguet, M., DeMets, C., ...  
686 Walpersdorf, A. (2016). Lateral Variations of Interplate Coupling along the  
687 Mexican Subduction Interface: Relationships with Long-Term Morphology and  
688 Fault Zone Mechanical Properties. *Pure and Applied Geophysics*, 173(10),  
689 3467–3486.
- 690 Ruff, L. J., & Tichelaar, B. W. (1996). What Controls the Seismogenic Plate In-  
691 terface in Subduction Zones? In *Geophysical monograph series* (pp. 105–111).  
692 American Geophysical Union.
- 693 Ryan, W. B. F., Carbotte, S. M., Coplan, J. O., O'Hara, S., Melkonian, A., Arko,  
694 R., ... Zemsky, R. (2009, March). Global Multi-Resolution Topography  
695 synthesis. *Geochemistry Geophysics Geosystems*, 10(3), n/a–n/a.
- 696 Sagiya, T. (1999). Interplate coupling in the Tokai District, central Japan, deduced  
697 from continuous GPS data. *Geophysical Research Letters*, 26(15), 2315–2318.
- 698 Saillard, M., Audin, L., Rousset, B., Avouac, J.-P., Chlieh, M., Hall, S. R., ... Far-  
699 ber, D. L. (2017, February). From the seismic cycle to long-term deformation:  
700 linking seismic coupling and Quaternary coastal geomorphology along the  
701 Andean megathrust. *Tectonics*, 36(2), 241–256.
- 702 Savage, J. C. (1983). A Dislocation Model of Strain Accumulation and Release at  
703 a Subduction Zone. *Journal of Geophysical Research-Solid Earth and Planets*,

- 704 88(NB6), 4984–4996.
- 705 Savage, J. C., & Thatcher, W. (1992). Interseismic Deformation at the Nankai  
706 Trough, Japan, Subduction Zone. *Journal of Geophysical Research-Solid Earth  
707 and Planets*, 97(B7), 11117–11135.
- 708 Sawai, Y., Satake, K., Kamataki, T., Nasu, H., Shishikura, M., Atwater, B. F., . . .  
709 Yamaguchi, M. (2004). Transient uplift after a 17th-century earthquake along  
710 the Kuril subduction zone. *Science*, 306(5703), 1918–1920.
- 711 Schmalzle, G. M., McCaffrey, R., & Creager, K. C. (2014, April). Central Casca-  
712 dia subduction zone creep. *Geochemistry Geophysics Geosystems*, 15(4), 1515–  
713 1532.
- 714 Seely, D. R., & Dickinson, W. R. (1977). Structure and stratigraphy of forearc re-  
715 gions. *AAPG Special Volumes*, A122, 1–23.
- 716 Sieh, K., Natawidjaja, D. H., Meltzner, A. J., Shen, C. C., Cheng, H., Li, K. S., . . .  
717 Edwards, R. L. (2008, December). Earthquake Supercycles Inferred from Sea-  
718 Level Changes Recorded in the Corals of West Sumatra. *Science*, 322(5908),  
719 1674–1678.
- 720 Simoes, M., Avouac, J.-P., Cattin, R., & Henry, P. (2004). The Sumatra subduction  
721 zone: A case for a locked fault zone extending into the mantle. *Journal of Geo-  
722 physical Research: Planets*, 109(B10).
- 723 Simons, M., Minson, S. E., Sladen, A., Ortega, F., Jiang, J., Owen, S. E., . . . Webb,  
724 F. H. (2011, June). The 2011 Magnitude 9.0 Tohoku-Oki Earthquake: Mo-  
725 saicking the Megathrust from Seconds to Centuries. *Science*, 332(6036),  
726 1421–1425.
- 727 Simpson, G. (2015). Accumulation of permanent deformation during earthquake cy-  
728 cles on reverse faults. *Journal of Geophysical Research*, 120, 1958–1974.
- 729 Snyder, N. P., Whipple, K. X., Tucker, G. E., & Merritts, D. J. (2002, June). In-  
730 teractions between onshore bedrock-channel incision and nearshore wave-base  
731 erosion forced by eustasy and tectonics. *Basin Research*, 14(2), 105–127.
- 732 Song, T.-R. A., & Simons, M. (2003, August). Large Trench-Parallel Gravity Vari-  
733 ations Predict Seismogenic Behavior in Subduction Zones. *Science*, 301(5633),  
734 630–633.
- 735 Spratt, R. M., & Lisiecki, L. E. (2016). A Late Pleistocene sea level stack. *Climate  
736 of the Past*, 12(4), 1079–1092.

- 737 Stevens, V. L., & Avouac, J.-P. (2015). Interseismic coupling on the main Himalayan  
738 thrust. *Geophysical Research Letters*, *42*(14), 5828–5837.
- 739 Sugiyama, Y. (1994). Neotectonics of Southwest Japan due to the right-oblique sub-  
740 duction of the Philippine Sea plate. *Geofísica Internacional*, *33*(1), 53–76.
- 741 Sun, T., Wang, K., & He, J. (2018, June). Crustal Deformation Following Great  
742 Subduction Earthquakes Controlled by Earthquake Size and Mantle Rheology.  
743 *Journal of Geophysical Research*, *123*(6), 5323–5345.
- 744 Sykes, L. R., Kisslinger, J. B., House, L., Davies, J. N., & Jacob, K. H. (1981). Rup-  
745 ture Zones and Repeat Times of Great Earthquakes Along the Alaska-Aleutian  
746 ARC, 1784–1980. In D. W. Simpson & P. G. Richards (Eds.), *Earthquake  
747 prediction an international review* (pp. 73–80). Washington, D. C.: American  
748 Geophysical Union.
- 749 Thatcher, W. (1984). The Earthquake Deformation Cycle at the Nankai Trough,  
750 Southwest Japan. *Journal of Geophysical Research-Solid Earth and Planets*,  
751 *89*(NB5), 3087–3101.
- 752 Trubienko, O., Fleitout, L., Garaud, J.-D., & Vigny, C. (2013, March). Interpreta-  
753 tion of interseismic deformations and the seismic cycle associated with large  
754 subduction earthquakes. *Tectonophysics*, *589*(C), 126–141.
- 755 Valensise, G., & Ward, S. N. (1991, October). Long-Term Uplift of the Santa-Cruz  
756 Coastline in Response to Repeated Earthquakes Along the San-Andreas Fault.  
757 *Bulletin of the Seismological Society of America*, *81*(5), 1694–1704.
- 758 van Dinther, Y., Gerya, T. V., Dalguer, L. A., Mai, P. M., Morra, G., & Giardini,  
759 D. (2013, December). The seismic cycle at subduction thrusts: Insights from  
760 seismo-thermo-mechanical models. *Journal of Geophysical Research*, *118*(12),  
761 6183–6202.
- 762 Vannucchi, P., Morgan, J. P., Silver, E. A., & Kluesner, J. W. (2016, June). Origin  
763 and dynamics of depositional subduction margins. *Geochemistry Geophysics  
764 Geosystems*, *17*(6), 1966–1974.
- 765 Vergne, J., Cattin, R., & Avouac, J.-P. (2001, September). On the use of disloca-  
766 tions to model interseismic strain and stress build-up at intracontinental thrust  
767 faults. *Geophysical Journal International*, *147*(1), 155–162.
- 768 Wallace, L. M. (2004). Subduction zone coupling and tectonic block rotations in the  
769 North Island, New Zealand. *Journal of Geophysical Research-Solid Earth and*

- 770 *Planets*, 109(B12), 477–21.
- 771 Wang, K., & Hu, Y. (2006, June). Accretionary prisms in subduction earthquake cy-  
 772 cles: The theory of dynamic Coulomb wedge. *Journal of Geophysical Research*,  
 773 111(B6), n/a–n/a.
- 774 Wang, K., & Tréhu, A. M. (2016, August). Invited review paper: Some outstanding  
 775 issues in the study of great megathrust earthquakes—The Cascadia example.  
 776 *Journal of Geodynamics*, 98, 1–18.
- 777 Wang, K., Wells, R., Mazzotti, S., Hyndman, R. D., & Sagiya, T. (2003, January).  
 778 A revised dislocation model of interseismic deformation of the Cascadia sub-  
 779 duction zone. *Journal of Geophysical Research*, 108(B1), 1085–13.
- 780 Wells, R. E., Blakely, R. J., Sugiyama, Y., Scholl, D. W., & Dinterman, P. A.  
 781 (2003). Basin-centered asperities in great subduction zone earthquakes: A  
 782 link between slip, subsidence, and subduction erosion? *Journal of Geophysical*  
 783 *Research: Planets*, 108(B10).
- 784 Willett, S. D., Beaumont, C., & Fullsack, P. (1993). Mechanical Model for the Tec-  
 785 tonics of Doubly Vergent Compressional Orogens. *Geology*, 21(4), 371–374.
- 786 Ye, L., Lay, T., & Kanamori, H. (2013, November). Large earthquake rupture pro-  
 787 cess variations on the Middle America megathrust. *Earth and Planetary Sci-*  
 788 *ence Letters*, 381(C), 147–155.
- 789 Yoshikawa, T. (1968, December). Seismic Crustal Deformation and its Relation to  
 790 Quaternary Tectonic Movement on the Pacific Coast of Southwest Japan. *The*  
 791 *Quaternary Research (Daiyonki-Kenkyu)*, 7(4), 157–170.
- 792 Yoshikawa, T., Kaizuka, S., & Ôta, Y. (1981). *The landforms of Japan* /. Tokyo:  
 793 University of Tokyo Press.
- 794 Yoshioka, S., Yabuki, T., Sagiya, T., Tada, T., & Matsu'ura, M. (1993). Interplate  
 795 coupling and relative plate motion in the Tokai district, central Japan, deduced  
 796 from geodetic data inversion using ABIC. *Geophysical Journal International*,  
 797 113, 607–621.
- 798 Yue, H., Lay, T., Rivera, L., An, C., Vigny, C., Tong, X., & Báez Soto, J. C. (2014,  
 799 October). Localized fault slip to the trench in the 2010 Maule, Chile  $M_w = 8.8$   
 800 earthquake from joint inversion of high-rate GPS, teleseismic body waves,  
 801 InSAR, campaign GPS, and tsunami observations. *Journal of Geophysical*  
 802 *Research*, 119(10), 7786–7804.

# Supporting Information for “Co-location of the downdip end of seismic locking and the continental shelf break”

Luca C. Malatesta<sup>1,2,3</sup>\*, Lucile Bruhat<sup>4</sup>, Noah J. Finnegan<sup>1</sup>, Jean-Arthur L.

Olive<sup>4</sup>

## Contents of this file

---

<sup>1</sup>Department of Earth and Planetary  
Sciences, University of California Santa  
Cruz, Santa Cruz, California, USA.

<sup>2</sup>Institute of Earth Surface Dynamics,  
University of Lausanne, Lausanne,  
Switzerland

<sup>3</sup>Earth Surface Process Modelling, GFZ  
German Research Center for Geosciences,  
Potsdam, Germany

<sup>4</sup>Department of Geology, École Normale  
Supérieure, Paris, France.

\*Corresponding author:

luca.malatesta@gfz-potsdam.de



1. Text S1
2. Text S2
3. Figures S1
4. Table S1
5. Table S2

### **Additional Supporting Information (Files uploaded separately)**

1. Description of *kml* file
2. Description for the three videos

### **Text S1: Selection criteria for the compilation**

We established selection criteria to use only the most reliable locking depth solutions in our global dataset. They are detailed below and supplementary Table S1 details which 21 inversions out of 48 total were selected.

Seismic ruptures need to be large enough to outline the downdip end of coupling ( $\sim M_w$  larger than 7, Lay et al., 2012). We ignore large seismic ruptures from historical catalogues that are only vaguely outlined and instead rely on ruptures that were heavily instrumented (Yue et al., 2014).

At sites where no large earthquake was recorded, coupling is determined based on interseismic deformation recorded by GNSS stations (located almost entirely onshore). In cases of well resolved co- and interseismic solutions, inversions from coseismic ruptures were selected over interseismic inversions. We select interseismic locking depth solutions if models can demonstrably resolve coupling offshore and if an agreement exists between different studies. Spatial resolution is mostly determined by the density and spatial dis-

tribution of geodetic measurements, and their associated uncertainties (Wang & Tréhu, 2016). Uncertainties over the locking depth estimate increase for wider continental shelves due larger separation between onshore stations and the locked region (e.g. LaFemina et al., 2009; Franco et al., 2012, in Central America). For lack of a simple selection criterion, we ignore locations where locking depth solutions derived from similar datasets by different authors vary greatly.

Four subduction zones are excluded from the reduced compilation because their geometry or coastal processes do not follow our conceptual model. The northern Kuril subduction, under Kamtchatka, dips steeply, placing arc volcanism so close to the trench that the margin is aggradational as volcanoes encroach on the sea (Bürgmann, 2005). The Gorda micro-plate in the southern Cascadia subduction zone is a very young oceanic plate ( $\sim 3$ Ma, Stock & Lee, 2010) whose slab deforms heavily under the active margin and the long-term interseismic deformation is likely to vary on a much faster timescale than that of the establishment of the submarine landscape. At the junction between Central and South America, vertical motion above the Costa Rica subduction zone is controlled by episodic forcings that reflect the subduction of structural and geological complexities (Edwards et al., 2018). Finally, the Colombian coastline is aggradational, as it appears that the sediment flux reaching the coast suffices to overcome coastal erosion and build land.

**Text S2: Numerical modelling** The numerical model used to illustrate the collocation of shelf break and locking depth while the coastline migrates landward is based on the work by Savage (1983) and Okada (1992) as implemented by Bruhat and Segall (2016) for interseismic deformation. A version of the Matlab code used for this manuscript is

available online as supplementary material. The parameters used to produce figures 5 A, B, and C are listed in Table S2. for coastal erosion and of

### **Data Set S1: Description of *kml* file**

The *kml* file attached to this contribution contains the traces of all locking depths imported from the literature (see Table SS1) and shelf break outlines as well as the positions of the profiles used to build Figure 4 and Figure S??.

### **Data Set S2: Description of MATLAB file file**

The MATLAB code attached to this contribution was used to produce the model runs of Figure 5 A, B, and C with the parameters listed in Table S2.

### **Movie S1:**

The three videos attached to this contribution show the model runs of Figure 5 A and with parameters listed in Table S2. The exact same simulations can be obtained with the MATLAB code attached.

### **Movie S2:**

The three videos attached to this contribution show the model runs of Figure 5 B and with parameters listed in Table S2. The exact same simulations can be obtained with the MATLAB code attached.

### **Movie S3:**

The three videos attached to this contribution show the model runs of Figure 5 C and with parameters listed in Table S2. The exact same simulations can be obtained with the MATLAB code attached.

## References

- Béjar-Pizarro, M., Socquet, A., Armijo, R., Carrizo, D., Genrich, J., & Simons, M. (2013, April). Andean structural control on interseismic coupling in the North Chile subduction zone. *Nature Geoscience*, *6*(6), 462–467.
- Briggs, R. W., Sieh, K., Meltzner, A. J., Natawidjaja, D. H., Galetzka, J., Suwargadi, B. W., ... Bock, Y. (2006). Deformation and slip along the Sunda Megathrust in the great 2005 Nias-Simeulue earthquake. *Science*, *311*(5769), 1897–1901.
- Bruhat, L., & Segall, P. (2016, November). Coupling on the northern Cascadia subduction zone from geodetic measurements and physics-based models. *Journal of Geophysical Research*, *121*(11), 8297–8314.
- Burgette, R. J., Weldon II, R. J., & Schmidt, D. A. (2009, January). Interseismic uplift rates for western Oregon and along-strike variation in locking on the Cascadia subduction zone. *Journal of Geophysical Research*, *114*(B1), TC3009–24.
- Bürgmann, R. (2005). Interseismic coupling and asperity distribution along the Kamchatka subduction zone. *Journal of Geophysical Research*, *110*(B7), 1675–17.
- Chlieh, M., Avouac, J.-P., Sieh, K., Natawidjaja, D. H., & Galetzka, J. (2008, May). Heterogeneous coupling of the Sumatran megathrust constrained by geodetic and paleogeodetic measurements. *Journal of Geophysical Research-Solid Earth and Planets*, *113*(B5), 2018–31.
- Chlieh, M., Perfettini, H., Tavera, H., Avouac, J.-P., Remy, D., Nocquet, J.-M., ... Bonvalot, S. (2011, December). Interseismic coupling and seismic potential along the Central Andes subduction zone. *Journal of Geophysical Research*, *116*(B12), B10404–21.

- Cross, R. S., & Freymueller, J. T. (2007, March). Plate coupling variation and block translation in the Andreanof segment of the Aleutian arc determined by subduction zone modeling using GPS data. *Geophysical Research Letters*, *34*(6), 1653–5.
- Edwards, J. H., Kluesner, J. W., Silver, E. A., & Bangs, N. L. (2018, February). Pleistocene vertical motions of the Costa Rican outer forearc from subducting topography and a migrating fracture zone triple junction. *Geosphere*, 1–25.
- Franco, A., Lasserre, C., Lyon-Caen, H., Kostoglodov, V., Molina, E., Guzman-Speziale, M., . . . Manea, V. C. (2012, April). Fault kinematics in northern Central America and coupling along the subduction interface of the Cocos Plate, from GPS data in Chiapas (Mexico), Guatemala and El Salvador. *Geophysical Journal International*, *189*(3), 1223–1236.
- Hashimoto, C., Noda, A., Sagiya, T., & Matsu'ura, M. (2009, January). Interplate seismogenic zones along the Kuril-Japan trench inferred from GPS data inversion. *Nature Geoscience*, *2*(2), 141–144.
- Hyndman, R. D., Wang, K., & Yamano, M. (1995, August). Thermal constraints on the seismogenic portion of the southwestern Japan subduction thrust. *Journal of Geophysical Research: Planets*, *100*(B8), 15373–15392.
- Johnson, J. M. (1998). Heterogeneous Coupling Along Alaska-Aleutians as Inferred From Tsunami, Seismic, and Geodetic Inversions. In *Tsunamigenic earthquakes and their consequences* (pp. 1–116). Elsevier.
- Johnson, J. M., Tanioka, Y., Ruff, L. J., Satake, K., Kanamori, H., & Sykes, L. R. (1994, December). The 1957 great Aleutian earthquake Pure Applied Geophysics, *142* (1), 1994, pp 3–28. *Pure and Applied Geophysics*, *142*(1), 3–28.

- Kanamori, H., & McNally, K. C. (1982, August). Variable rupture mode of the subduction zone along the Ecuador-Colombia coast. *Bulletin of the Seismological Society of America*, *72*(4), 1241–1253.
- LaFemina, P., Dixon, T. H., Govers, R., Norabuena, E., Turner, H., Saballos, A., ... Strauch, W. (2009, May). Fore-arc motion and Cocos Ridge collision in Central America. *Geochemistry Geophysics Geosystems*, *10*(5), n/a–n/a.
- Lay, T., Ammon, C. J., Kanamori, H., Xue, L., & Kim, M. J. (2011, September). Possible large near-trench slip during the 2011  $M_w$ 9.0 off the Pacific coast of Tohoku Earthquake. *Earth, Planets and Space*, *63*(7), 687–692.
- Lay, T., Kanamori, H., Ammon, C. J., Koper, K. D., Hutko, A. R., Ye, L., ... Rushing, T. M. (2012, April). Depth-varying rupture properties of subduction zone megathrust faults. *Journal of Geophysical Research*, *117*(B4), n/a–n/a.
- Lay, T., Yue, H., Brodsky, E. E., & An, C. (2014, June). The 1 April 2014 Iquique, Chile,  $M_w$ 8.1 earthquake rupture sequence. *Geophysical Research Letters*, *41*(11), 3818–3825.
- Li, L., Lay, T., Cheung, K. F., & Ye, L. (2016, May). Joint modeling of teleseismic and tsunami wave observations to constrain the 16 September 2015 Illapel, Chile,  $M_w$ 8.3 earthquake rupture process. *Geophysical Research Letters*, *43*(9), 4303–4312.
- Loveless, J. P., & Meade, B. J. (2010, February). Geodetic imaging of plate motions, slip rates, and partitioning of deformation in Japan. *Journal of Geophysical Research*, *115*(B2), L11303–35.
- McCaffrey, R., Qamar, A. I., King, R. W., Wells, R., Khazaradze, G., Williams, C. A., ... Zwick, P. C. (2007, June). Fault locking, block rotation and crustal deformation

in the Pacific Northwest. *Geophysical Journal International*, 169(3), 1315–1340.

Metois, M., Socquet, A., & Vigny, C. (2012, March). Interseismic coupling, segmentation and mechanical behavior of the central Chile subduction zone. *Journal of Geophysical Research*, 117(B3), 40–16.

Metois, M., Vigny, C., & Socquet, A. (2016, April). Interseismic Coupling, Megathrust Earthquakes and Seismic Swarms Along the Chilean Subduction Zone (38°–18°S). *Pure and Applied Geophysics*, 173(5), 1431–1449.

Metois, M., Vigny, C., Socquet, A., Delorme, A., Morvan, S., Ortega, I., & Valderas-Bermejo, C. M. (2013, November). GPS-derived interseismic coupling on the subduction and seismic hazards in the Atacama region, Chile. *Geophysical Journal International*, 196(2), 644–655.

Natawidjaja, D. H., Sieh, K., Galetzka, J., Suwargadi, B. W., Cheng, H., Edwards, R. L., & Chlieh, M. (2007, February). Interseismic deformation above the Sunda Megathrust recorded in coral microatolls of the Mentawai islands, West Sumatra. *Journal of Geophysical Research-Solid Earth and Planets*, 112(B2), 1897–27.

Nocquet, J.-M., Villegas-Lanza, J. C., Chlieh, M., Mothes, P. A., Rolandone, F., Jarriin, P., ... Yepes, H. (2014, March). Motion of continental slivers and creeping subduction in the northern Andes. *Nature Geoscience*, 7(4), 287–291.

Okada, Y. (1992, April). Internal deformation due to shear and tensile faults in a half-space. *Bulletin of the Seismological Society of America*, 82(2), 1018–1040.

Park, J.-O., Tsuru, T., Kodaira, S., Cummins, P. R., & Kaneda, Y. (2002, August). Splay Fault Branching Along the Nankai Subduction Zone. *Science*, 297(5584), 1157–1160.

- Radiguet, M., Cotton, F., Vergnolle, M., Campillo, M., Walpersdorf, A., Cotte, N., & Kostoglodov, V. (2012, April). Slow slip events and strain accumulation in the Guerrero gap, Mexico. *Journal of Geophysical Research*, *117*(B4), n/a–n/a.
- Saillard, M., Audin, L., Rousset, B., Avouac, J.-P., Chlieh, M., Hall, S. R., . . . Farber, D. L. (2017, February). From the seismic cycle to long-term deformation: linking seismic coupling and Quaternary coastal geomorphology along the Andean megathrust. *Tectonics*, *36*(2), 241–256.
- Savage, J. C. (1983). A Dislocation Model of Strain Accumulation and Release at a Subduction Zone. *Journal of Geophysical Research-Solid Earth and Planets*, *88*(NB6), 4984–4996.
- Schmalzle, G. M., McCaffrey, R., & Creager, K. C. (2014, April). Central Cascadia subduction zone creep. *Geochemistry Geophysics Geosystems*, *15*(4), 1515–1532.
- Stock, J. M., & Lee, J. (2010, July). Do microplates in subduction zones leave a geological record? *Tectonics*, *13*(6), 1472–1487.
- Sykes, L. R., Kisslinger, J. B., House, L., Davies, J. N., & Jacob, K. H. (1981). Rupture Zones and Repeat Times of Great Earthquakes Along the Alaska-Aleutian ARC, 1784–1980. In D. W. Simpson & P. G. Richards (Eds.), *Earthquake prediction an international review* (pp. 73–80). Washington, D. C.: American Geophysical Union.
- Wallace, L. M. (2004). Subduction zone coupling and tectonic block rotations in the North Island, New Zealand. *Journal of Geophysical Research-Solid Earth and Planets*, *109*(B12), 477–21.
- Wang, K., & Tréhu, A. M. (2016, August). Invited review paper: Some outstanding issues in the study of great megathrust earthquakes—The Cascadia example. *Journal of*



*Geodynamics*, 98, 1–18.

Wang, K., Wells, R., Mazzotti, S., Hyndman, R. D., & Sagiya, T. (2003, January).

A revised dislocation model of interseismic deformation of the Cascadia subduction zone. *Journal of Geophysical Research*, 108(B1), 1085–13.

Ye, L., Lay, T., & Kanamori, H. (2013, November). Large earthquake rupture process

variations on the Middle America megathrust. *Earth and Planetary Science Letters*, 381(C), 147–155.

Yue, H., Lay, T., Rivera, L., An, C., Vigny, C., Tong, X., & Báez Soto, J. C. (2014,

October). Localized fault slip to the trench in the 2010 Maule, Chile  $M_w = 8.8$  earthquake from joint inversion of high-rate GPS, teleseismic body waves, InSAR, campaign GPS, and tsunami observations. *Journal of Geophysical Research*, 119(10), 7786–7804.

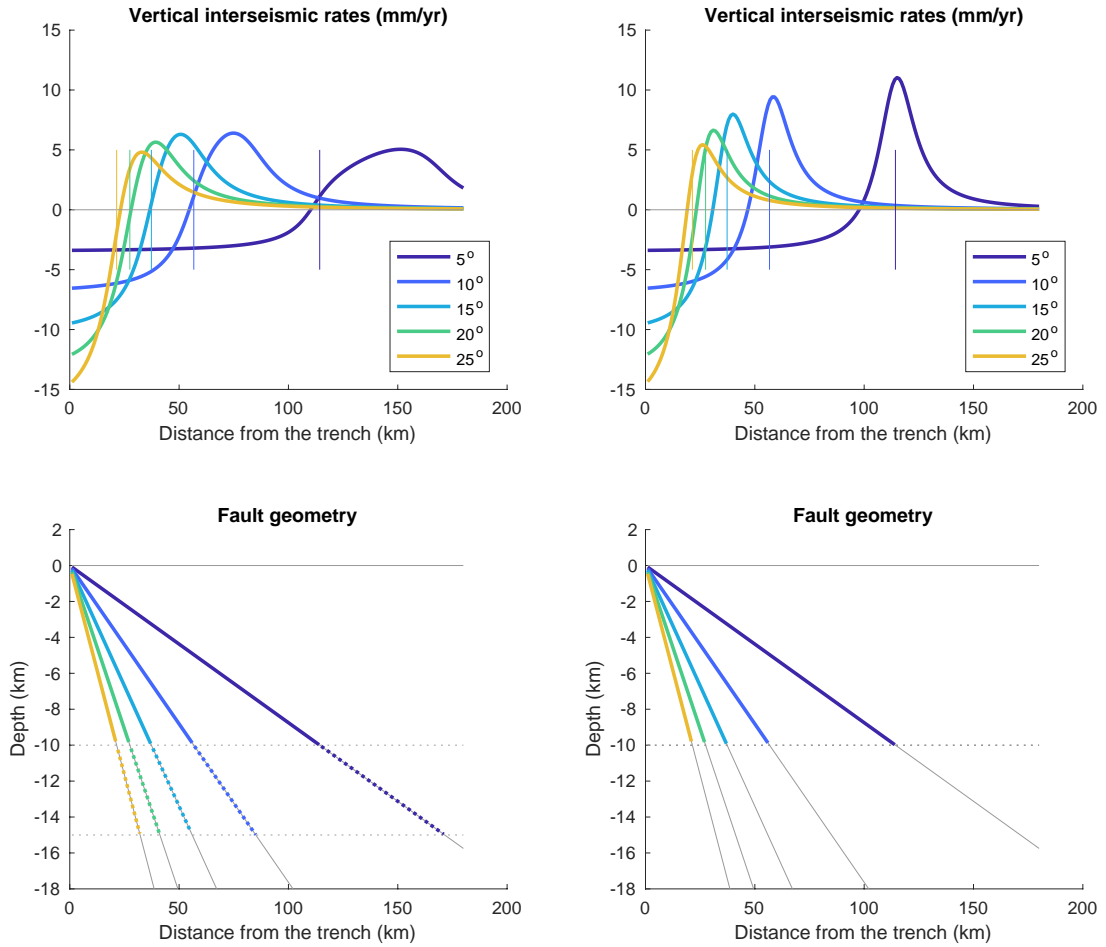


**Figure S1.** Left: relationship between the uplift hinge line and the locking depth for a fault with transitional locking (from 10 to 15 km) at varying dip angles. Right: same as left but without transitional locking. The uplift hinge line is most removed from the position of the locking depth for gently sloping faults without transitional locking. A zone of transitional locking is however expected in most if not all locations.

February 12, 2020, 8:29pm

Table S1: continued from previous page.

| Subduction<br>transect | Lat./Lon. | Dist. trench to... [km] |       |         |  | Method | Reference | Selection |
|------------------------|-----------|-------------------------|-------|---------|--|--------|-----------|-----------|
|                        |           | shelf                   | coast | locking |  |        |           |           |

Table S1: List of measurements on profiles across subduction zones. The latitude/longitude coordinates indicate the intersection between profile and subduction trench (or deformation front). The Method column reflects if locking depth is identified from inversion of GPS or leveling (LVL) data, from slab isotherms (isoT), or from the inversion of coseismic ruptures (EQ). The selection columns reflects whether the solution was selected for Figure 4 of the main text along side a rationale for the choice: *creep*, the fault is creeping; *co>inter*: coseismic solutions are favored over interseismic ones (also used for all profiles of subductions where one resolved coseismic rupture contradicts an interseismic solution); *isoT*, solutions based on isotherm estimates are ignored; *default*, best solution and others are ignored; *volc. coast*, the coast is not erosional but built up by volcanoes; *island*, the coastline is offset from the continent by an island; *tecto.*, local tectonics deviate strongly from a standard subduction geometry (due to strike-slip components, slab age or dip angle); *equiv.*, one solution is picked among equivalent ones; *resolut.*, the resolution of the inversion is too low; *deposit.*, the coast is not erosional but built up by sediments; *contrad.*, different solutions contradict each other.

Table S1: continued from previous page.

| Subduction<br>transect | Lat./Lon.     | Dist. trench to... [km] |       |         | Method | Reference  | Selection      |
|------------------------|---------------|-------------------------|-------|---------|--------|--|----------------|
|                        |               | shelf                   | coast | locking |        |  |                |
| Hikurangi 2            | -39.80/178.63 | 70                      | 151   | 12      | GPS    | Wallace (2004)   | No (creep)     |
| Hikurangi 3            | -38.51/179.11 | 40                      | 72    | 5       | GPS    | Wallace (2004)   | No (creep)     |
| Sumatra 1              | -4.28/100.18  | 170                     | 232   | 164     | GPS    | Chlieh, Avouac, Sieh, Natawidjaja, and Galetzka (2008) | No (co>inter)  |
| "                      | "             | "                       | "     | 170     | EQ     | Natawidjaja et al. (2007)                              | Yes (co>inter) |
| Sumatra 2              | -2.42/98.65   | 221                     | 237   | 190     | GPS    | Chlieh et al. (2008)                                   | No (co>inter)  |
| "                      | "             | "                       | "     | 202     | EQ     | Natawidjaja et al. (2007)                              | Yes (co>inter) |
| Sumatra 3              | 0.76/96.81    | 185                     | 201   | 145     | GPS    | Chlieh et al. (2008)                                   | No (co>inter)  |
| "                      | "             | "                       | "     | 213     | EQ     | Briggs et al. (2006)                                   | Yes (co>inter) |
| Nankai 1               | 32.03/134.37  | 152                     | 180   | 145     | isoT   | Hyndman, Wang, and Yamano (1995)                       | No (isoT)      |
| "                      | "             | "                       | "     | 213     | GPS    | Loveless and Meade (2010)                              | No (co>inter)  |
| Nankai 2               | 32.74/136.10  | 81                      | 88    | 83      | isoT   | Hyndman et al. (1995)                                  | No (isoT)      |
| "                      | "             | "                       | "     | 128     | GPS    | Loveless and Meade (2010)                              | No (co>inter)  |
| Nankai 3               | 33.18/137.22  | 123                     | 132   | 110     | isoT   | Hyndman et al. (1995)                                  | No (isoT)      |
| "                      | "             | "                       | "     | 151     | GPS    | Loveless and Meade (2010)                              | No (co>inter)  |
| "                      | "             | "                       | "     | 130     | EQ     | Park, Tsuru, Kodaira, Cummins, and Kaneda (2002)       | Yes (co>inter) |

February 12, 2020, 8:29pm

Table S1: continued from previous page.

| Subduction<br>transect | Lat./Lon.    | Dist. trench to... [km] |       |         | Method | Reference                                     | Selection      |
|------------------------|--------------|-------------------------|-------|---------|--------|---|----------------|
|                        |              | shelf                   | coast | locking |        |   |                |
| N. Honshu 1            | 35.24/142.22 | 101                     | 133   | 154     | isoT   | Hyndman et al. (1995)                         | No (isoT)      |
| "                      | "            | "                       | "     | 81      | GPS    | Loveless and Meade (2010)                     | No (co>inter)  |
| N. Honshu 2            | 37.34/143.72 | 190                     | 242   | 199     | isoT   | Hyndman et al. (1995)                         | No (co>inter)  |
| "                      | "            | "                       | "     | 218     | GPS    | Loveless and Meade (2010)                     | No (co>inter)  |
| "                      | "            | "                       | "     | 227     | GPS    | Hashimoto, Noda, Sagiya, and Matsu'ura (2009) | No (co>inter)  |
| "                      | "            | "                       | "     | 196     | EQ     | Lay, Ammon, Kanamori, Xue, and Kim (2011)     | Yes (co>inter) |
| N. Honshu 3            | 39.96/144.33 | 184                     | 211   | 175     | isoT   | Hyndman et al. (1995)                         | No (isoT)      |
| "                      | "            | "                       | "     | 154     | GPS    | Hashimoto et al. (2009)                       | Yes (default)  |
| N. Honshu 4            | 40.61/144.53 | 325                     | 406   | 197     | isoT   | Hyndman et al. (1995)                         | No (isoT)      |
| "                      | "            | "                       | "     | 263     | GPS    | Loveless and Meade (2010)                     | No (co>inter)  |
| "                      | "            | "                       | "     | 246     | GPS    | Hashimoto et al. (2009)                       | Yes (default)  |
| Hokkaido 1             | 41.30/145.14 | 174                     | 198   | 161     | isoT   | Hyndman et al. (1995)                         | No (isoT)      |
| "                      | "            | "                       | "     | 191     | GPS    | Loveless and Meade (2010)                     | No (co>inter)  |
| "                      | "            | "                       | "     | 186     | GPS    | Hashimoto et al. (2009)                       | Yes (default)  |
| Hokkaido 2             | 41.88/146.43 | 138                     | 171   | 155     | isoT   | Hyndman et al. (1995)                         | No (isoT)      |
| "                      | "            | "                       | "     | 182     | GPS    | Loveless and Meade (2010)                     | No (co>inter)  |

February 12, 2020, 8:29pm

Table S1: continued from previous page.

| Subduction<br>transect | Lat./Lon.     | Dist. trench to... [km] |       |         | Method | Reference  | Selection        |
|------------------------|---------------|-------------------------|-------|---------|--------|--|------------------|
|                        |               | shelf                   | coast | locking |        |  |                  |
| "                      | "             | "                       | "     | 172     | GPS    | Hashimoto et al. (2009)                            | Yes (default)    |
| Kamchatka 1            | 51.12/160.26  | 144                     | 167   | 174     | GPS    | Bürgmann (2005)                                    | No (volc. coast) |
| Kamchatka 2            | 53.36/162.62  | 153                     | 188   | 140     | GPS    | Bürgmann (2005)                                    | No (volc. coast) |
| Kamchatka 3            | 54.87/163.68  | 129                     | 144   | 37      | GPS    | Bürgmann (2005)                                    | No (volc. coast) |
| Aleutian 1             | 50.39/177.95  | 132                     | 141   | 89      | GPS    | Cross and Freymueller (2007)                       | No (co>inter)    |
| "                      | "             | "                       | "     | 119     | EQ     | Johnson et al. (1994)                              | Yes (co>inter)   |
| Aleutian 2             | 50.56/-175.43 | 133                     | 157   | 107     | GPS    | Cross and Freymueller (2007)                       | No (co>inter)    |
| "                      | "             | "                       | "     | 138     | EQ     | Johnson et al. (1994)                              | Yes (co>inter)   |
| Aleutian 3             | 50.72/-173.64 | 133                     | 161   | 68      | GPS    | Cross and Freymueller (2007)                       | No (co>inter)    |
| "                      | "             | "                       | "     | 153     | EQ     | Johnson et al. (1994)                              | Yes (co>inter)   |
| Alaska 1               | 54.28/-156.82 | 189                     | 228   | 185     | EQ     | Johnson (1998)                                     | Yes (default)    |
| Alaska 2               | 56.18/-151.56 | 138                     | 138   | 212     | EQ     | Sykes, Kisslinger, House, Davies, and Jacob (1981) | No (island)      |
| Alaska 3               | 57.25/-148.56 | 283                     | 384   | 266     | EQ     | Sykes et al. (1981)                                | Yes (default)    |
| Alaska 4               | 58.83/-146.18 | 139                     | 139   | 261     | EQ     | Sykes et al. (1981)                                | No (tecto.)      |

February 12, 2020, 8:29pm

Table S1: continued from previous page.

| Subduction<br>transect | Lat./Lon.      | Dist. trench to... [km] |       |         | Method | Reference   | Selection    |
|------------------------|----------------|-------------------------|-------|---------|--------|---|--------------|
|                        |                | shelf                   | coast | locking |        |   |              |
| Cascadia 1             | 48.43/-126.85  | 53                      | 101   | 48      | GPS    | Wang, Wells, Mazzotti, Hyndman, and Sagiya (2003) | No (equiv.)  |
| "                      | "              | "                       | "     | 50      | GPS    | McCaffrey et al. (2007)                           | No (equiv.)  |
| "                      | "              | "                       | "     | 50      | GPS    | Schmalzle, McCaffrey, and Creager (2014)          | Yes (equiv.) |
| Cascadia 2             | 46.67/-125.89  | 83                      | 137   | 81      | GPS    | Wang et al. (2003)                                | No (equiv.)  |
| "                      | "              | "                       | "     | 50      | GPS    | McCaffrey et al. (2007)                           | No (equiv.)  |
| "                      | "              | "                       | "     | 94      | GPS    | Schmalzle et al. (2014)                           | Yes (equiv.) |
| Cascadia 3             | 44.33/-125.33  | 38                      | 98    | 39      | GPS    | Wang et al. (2003)                                | No (equiv.)  |
| "                      | "              | "                       | "     | 50      | GPS    | McCaffrey et al. (2007)                           | No (equiv.)  |
| "                      | "              | "                       | "     | 42      | GPS    | Schmalzle et al. (2014)                           | No (equiv.)  |
| "                      | "              | "                       | "     | 34      | LVL    | Burgette, Weldon II, and Schmidt (2009)           | Yes (equiv.) |
| Cascadia 4             | 42.017/-125.27 | 58                      | 89    | 43      | GPS    | Wang et al. (2003)                                | No (tecto.)  |
| "                      | "              | "                       | "     | 50      | GPS    | McCaffrey et al. (2007)                           | No (tecto.)  |
| "                      | "              | "                       | "     | 45      | GPS    | Schmalzle et al. (2014)                           | No (tecto.)  |
| "                      | "              | "                       | "     | 49      | LVL    | Burgette et al. (2009)                            | No (tecto.)  |
| Mexico 1               | 17.54/-103.17  | 62                      | 72    | 83      | EQ     | Radiguet et al. (2012)                            | No (tecto.)  |
| Mexico 2               | 16.16/-99.69   | 47                      | 61    | 87      | EQ     | Radiguet et al. (2012)                            | No (tecto.)  |

February 12, 2020, 8:29pm



Table S1: continued from previous page.

| Subduction<br>transect | Lat./Lon.    | Dist. trench to... [km] |       |         | Method | Reference                    | Selection     |
|------------------------|--------------|-------------------------|-------|---------|--------|------------------------------|---------------|
|                        |              | shelf                   | coast | locking |        |                              |               |
| Mexico 3               | 15.30/-96.95 | 45                      | 50    | 88      | EQ     | Radiguet et al. (2012)       | No (tect.)    |
| Mexico 4               | 14.43/-94.39 | 67                      | 173   | 54      | GPS    | Franco et al. (2012)         | No (resolut.) |
| GTM to NIC 1           | 13.31/-92.35 | 65                      | 115   | 38      | GPS    | LaFemina et al. (2009)       | No (resolut.) |
| "                      | "            | "                       | "     | 80      | EQ     | Ye, Lay, and Kanamori (2013) | Yes (default) |
| GTM to NIC 2           | 11.84/-88.79 | 72                      | 160   | 27      | GPS    | LaFemina et al. (2009)       | No (resolut.) |
| "                      | "            | "                       | "     | 75      | EQ     | Ye et al. (2013)             | Yes (default) |
| GTM to NIC 3           | 10.95/-87.33 | 55                      | 128   | 18      | GPS    | LaFemina et al. (2009)       | No (resolut.) |
| "                      | "            | "                       | "     | 86      | EQ     | Ye et al. (2013)             | Yes (default) |
| Costa Rica 1           | 9.41/-85.92  | 50                      | 67    | 114     | GPS    | LaFemina et al. (2009)       | No (tect.)    |
| "                      | "            | "                       | "     | 111     | EQ     | Ye et al. (2013)             | No (tect.)    |
| Costa Rica 2           | 8.57/-84.27  | 36                      | 87    | 22      | GPS    | LaFemina et al. (2009)       | No (tect.)    |
| Costa Rica 3           | 8.23/-83.48  | 20                      | 24    | 53      | GPS    | LaFemina et al. (2009)       | No (tect.)    |
| COL - ECD 1            | 3.83/-78.58  | 99                      | 136   | 148     | EQ     | Kanamori and McNally (1982)  | No (deposit.) |
| COL - ECD 2            | 1.74/-79.95  | 86                      | 113   | 132     | EQ     | Kanamori and McNally (1982)  | No (deposit.) |

February 12, 2020, 8:29pm

Table S1: continued from previous page.

| Subduction<br>transect | Lat./Lon.     | Dist. trench to... [km] |       |         | Method | Reference                         | Selection      |
|------------------------|---------------|-------------------------|-------|---------|--------|-----------------------------------|----------------|
|                        |               | shelf                   | coast | locking |        |                                   |                |
| "                      | "             | "                       | "     | 74      | GPS    | Nocquet et al. (2014)             | No (deposit.)  |
| COL - ECD 3            | -0.03/-80.99  | 30                      | 70    | 113     | EQ     | Kanamori and McNally (1982)       | No (deposit.)  |
| "                      | "             | "                       | "     | 67      | GPS    | Nocquet et al. (2014)             | No (deposit.)  |
| Peru 1                 | -9.01/-80.81  | 115                     | 220   | 47      | GPS    | Nocquet et al. (2014)             | No (resolut.)  |
| Peru 2                 | -12.92/-78.34 | 124                     | 165   | 200     | GPS    | Nocquet et al. (2014)             | No (resolut.)  |
| Peru 3                 | -17.78/-73.78 | 105                     | 115   | 164     | GPS    | Chlieh et al. (2011)              | No (resolut.)  |
| Peru 4                 | -19.15/-71.85 | 158                     | 172   | 80      | GPS    | Chlieh et al. (2011)              | No (resolut.)  |
| Chile 1                | -19.90/-71.39 | 123                     | 132   | 119     | GPS    | Chlieh et al. (2011)              | No (co>inter)  |
| "                      | "             | "                       | "     | 160     | GPS    | Metois, Vigny, and Socquet (2016) | No (co>inter)  |
| "                      | "             | "                       | "     | 116     | EQ     | Lay, Yue, Brodsky, and An (2014)  | Yes (co>inter) |
| Chile 2                | -23.12/-71.26 | 68                      | 72    | 156     | GPS    | Chlieh et al. (2011)              | No (contrad.)  |
| "                      | "             | "                       | "     | 133     | GPS    | Metois et al. (2016)              | No (contrad.)  |
| "                      | "             | "                       | "     | 70      | GPS    | Saillard et al. (2017)            | No (contrad.)  |
| "                      | "             | "                       | "     | 71      | GPS    | Béjar-Pizarro et al. (2013)       | No (contrad.)  |
| Chile 3                | -26.34/-71.62 | 81                      | 98    | 96      | GPS    | Metois et al. (2013)              | No (contrad.)  |

February 12, 2020, 8:29pm

Table S1: continued from previous page.

| Subduction<br>transect | Lat./Lon.     | Dist. trench to... [km] |       |         | Method | Reference                         | Selection      |
|------------------------|---------------|-------------------------|-------|---------|--------|-----------------------------------|----------------|
|                        |               | shelf                   | coast | locking |        |                                   |                |
| "                      | "             | "                       | "     | 172     | GPS    | Metois et al. (2016)              | No (contrad.)  |
| "                      | "             | "                       | "     | 123     | GPS    | Saillard et al. (2017)            | No (contrad.)  |
| "                      | "             | "                       | "     | 113     | GPS    | Metois, Socquet, and Vigny (2012) | No (contrad.)  |
| Chile 4                | -31.14/-72.59 | 85                      | 89    | 93      | GPS    | Metois et al. (2013)              | No (co>inter)  |
| "                      | "             | "                       | "     | 113     | GPS    | Metois et al. (2016)              | No (co>inter)  |
| "                      | "             | "                       | "     | 101     | GPS    | Saillard et al. (2017)            | No (co>inter)  |
| "                      | "             | "                       | "     | 95      | GPS    | Metois et al. (2012)              | No (co>inter)  |
| "                      | "             | "                       | "     | 84      | EQ     | Yue et al. (2014)                 | Yes (co>inter) |
| Chile 5                | -34.48/-73.50 | 119                     | 134   | 140     | GPS    | Metois et al. (2012)              | No (co>inter)  |
| "                      | "             | "                       | "     | 181     | GPS    | Saillard et al. (2017)            | No (co>inter)  |
| "                      | "             | "                       | "     | 144     | GPS    | Metois et al. (2016)              | No (co>inter)  |
| "                      | "             | "                       | "     | 113     | EQ     | Li, Lay, Cheung, and Ye (2016)    | Yes (co>inter) |

February 12, 2020, 8:29pm

**Table S2.** Numerical model parameters for simulations shown in Figure 5 A, B,, and C.

| <b>Parameters:</b>                            | <b>Values:</b>             |
|---|----------------------------|
| depth of trench <b>ztrench</b>                | 2.5 [km]                   |
| plate rate <b>srate</b>                       | 2 [mm/yr]                  |
| locking depth <b>zlock</b>                    | 10 [km]                    |
| transition depth <b>ztrans</b>                | 15 [km]                    |
| non-recoverable interseismic deformation      | 5% of total                |
| megathrust dip <b>dip</b>                     | 12 [°]                     |
| offshore wave power <b>P_off</b>              | $5 \times 10^{-2}$         |
| power expended in shallowest water <b>P_0</b> | $5 \times 10^{-5}$         |
| depth of wave base <b>dwb</b>                 | 100 [m]                    |
| <u>Reference case, 5A:</u>                    |                            |
| incision coefficient <b>b_i</b>               | $1.3 \times 10^{-5}$ [m/J] |
| cliff retreat coefficient <b>b_c</b>          | $2.3 \times 10^{-6}$ [m/J] |
| max. isostatic uplift <b>u_isostatic</b>      | 0.4 [mm/yr]                |
| <u>Subsidence case, 5B:</u>                   |                            |
| incision coefficient <b>b_i</b>               | $7 \times 10^{-6}$ [m/J]   |
| cliff retreat coefficient <b>b_c</b>          | $5 \times 10^{-7}$ [m/J]   |
| max. isostatic uplift <b>u_isostatic</b>      | 0.4 [mm/yr]                |
| max. subsidence rate <b>u_subsid</b>          | 1 [mm/yr]                  |
| width of forearc basin <b>farc_width</b>      | 75 [km]                    |
| <u>Narrow case, 5C:</u>                       |                            |
| incision coefficient <b>b_i</b>               | $7.5 \times 10^{-6}$ [m/J] |
| cliff retreat coefficient <b>b_c</b>          | $1.2 \times 10^{-6}$ [m/J] |
| max. isostatic uplift <b>u_isostatic</b>      | 2 [mm/yr]                  |